Electron and muon anomalous magnetic moments in the $\mathbb{Z}_3$-NMSSM

Junjie Cao[1,2,*] Lei Meng[1,†] and Yuanfang Yue[1,‡]

[1]*Department of Physics, Henan Normal University, Xinxiang 453007, China*
[2]*Schools of Physics, Shandong University, Jinan, Shandong 250100, China*

Inspired by the recent measurements of the muon and electron anomalous magnetic moments, the rapid progress of the LHC search for supersymmetry, and the significantly improved sensitivities of dark matter direct detection experiments, we studied the supersymmetric contribution to the electron $g-2$, a_e^{SUSY}, in the Next-to-Minimal Supersymmetric Standard Model with a discrete $\mathbb{Z}_3$ symmetry. We concluded that a_e^{SUSY} was mainly correlated with a_μ^{SUSY} by the formula $a_e^{\text{SUSY}}/m_e^2 \simeq a_\mu^{\text{SUSY}}/m_\mu^2$, and significant violations of this correlation might occur only in rare cases. As a result, a_e^{SUSY} was typically around 5×10^{-14} when $a_\mu^{\text{SUSY}} \simeq 2.5 \times 10^{-9}$. We also concluded that the dark matter direct detection and LHC experiments played crucial roles in determining the maximum reach of a_e^{SUSY}. Concretely, a_e^{SUSY} might be around 3×10^{-13} in the optimum cases if one used the XENON-1T experiment to limit the supersymmetry parameter space. This prediction, however, was reduced to 1.5×10^{-13} after implementing the LZ restrictions and 1.0×10^{-13} when further considering the LHC restrictions.

I. INTRODUCTION

The anomalous magnetic moment of leptons, $a_l \equiv g_l - 2$, is one of the most accurate measurements in particle physics. In 2021, the E989 experiment at FermiLab published its first result of the muon anomalous magnetic moment [1], which was consistent with the previous measurement of the Brookhaven National Laboratory (BNL) E821 experiment [2,3]. The combined result revealed a 4.2σ deviation from the prediction of the Standard Model (SM) [4–23]:

$$\Delta a_\mu \equiv a_\mu^{\text{Exp}} - a_\mu^{\text{SM}} = (25.1 \pm 5.9) \times 10^{-10}, \quad (1.1)$$

if the recent lattice calculations of the hadron vacuum polarization (HVP) were ignored [24–26].[1] Remarkably, the uncertainty in Δa_μ will significantly reduce in the coming times when more experimental data from ongoing

experiments at Fermilab [31] and future experiments at JPARC [32] are available. As a result, a more than 5σ deviation may be achieved if the central values of a_μ^{SM} and a_μ^{Exp} remain unchanged, which will serve as a robust evidence of new physics beyond the SM (BSM). In addition, the measurement of the fine structure constant by the Laboratoire Kastler Brossel (LKB) using ^{87}Rb atoms [33] concluded a positive difference of 1.6σ between the experimental measurement and the SM prediction of electron anomalous magnetic moment [34]:

$$\Delta a_e^{\text{Rb}} \equiv a_e^{\text{Exp,Rb}} - a_e^{\text{SM}} = (4.8 \pm 3.0) \times 10^{-13}, \quad (1.2)$$

while that by the Lawrence Berkeley National Laboratory (LBNL) using the ^{133}Cs atom obtained a negative difference of 2.4σ [35]:

$$\Delta a_e^{\text{Cs}} \equiv a_e^{\text{Exp,Cs}} - a_e^{\text{SM}} = (-8.7 \pm 3.6) \times 10^{-13}. \quad (1.3)$$

Although the two results differ by more than 5σ for still unknown reasons [33], they all indicate a sizable deviation from a_e^{SM} and thus, like the muon $g-2$ anomaly, hint at the BSM physics' existence.

To date, the muon $g-2$ anomaly has been intensively studied, which was recently reviewed in Refs. [3,36]. In contrast, only a few unified explanations of the electron and muon anomalies were investigated in the extensions of the SM with $SU(2)_L$ singlet or doublet Higgs bosons [37–59], vectorlike fermions [60–70], leptoquarks [71–74], different seesaw mechanisms [75–80], and new gauge

*junjiec@alumni.itp.ac.cn
†mel18@foxmail.com
‡yueyuanfang@htu.edu.cn
[1]Roughly speaking, these calculations can mitigate the discrepancy [3]. However, they are in tensions with the HVP contribution extracted from the e^+e^- data and the global fit of the precision electroweak observations [27–30].

symmetries [81–89], respectively, and their supersymmetric versions [90–103]. The anomalies were also studied in the effective Lagrangian framework [104]. These works revealed that explaining the two anomalies together in the same new physical model was challenging if there were no flavor mixings in the lepton part. This is because the BSM contribution to the lepton anomalous magnetic moment can be decomposed as the square of the lepton mass multiplied by the factor R_ℓ in the flavor conserving case. Equations (1.1)–(1.3) then indicate that R_ℓ for electron and muon are

$$R_e^{\rm Rb} \equiv \frac{\Delta a_e^{\rm Rb}}{m_e^2} = 1.85 \times 10^{-6}~{\rm GeV}^{-2}, \qquad (1.4)$$

$$R_e^{\rm Cs} \equiv \frac{\Delta a_e^{\rm Cs}}{m_e^2} = -3.34 \times 10^{-6}~{\rm GeV}^{-2}, \qquad (1.5)$$

$$R_\mu \equiv \frac{\Delta a_\mu}{m_\mu^2} = 2.25 \times 10^{-7}~{\rm GeV}^{-2}, \qquad (1.6)$$

respectively. Since $|R_e|$ is at least 7 times larger than R_μ, it is difficult to explain the two anomalies by a common physical origin. In the following, we concentrate on $\Delta a_e^{\rm Rb}$ instead of $\Delta a_e^{\rm Cs}$ in seeking the common origin due to the following two considerations. One is that given $|\Delta a_e^{\rm Cs}| > \Delta a_e^{\rm Rb}$, explaining the $^{133}C_s$ result prefers lighter new particles, which contribute to the electron moment, and/or more robust couplings of these particles to an electron in comparison with explaining the $^{87}R_b$ result. Consequently, the Cesium explanation is more tightly limited by current experiments. The other is that Δa_e and Δa_μ are usually of the same sign if they have a similar physical origin. Given $\Delta a_\mu \sim 25.1 \times 10^{-10}$, it is hard to predict a negative Δa_e.

Among the new physics theories that can provide a consistent description of the leptonic anomalies, the minimal realizations of supersymmetry (SUSY) are most attractive due to their elegant theoretical structure and capabilities of naturally solving many problems of the SM, such as the hierarchy problem, the unification of the three forces, and the mystery of dark matter (DM) [105–110]. Studies of the muon $g-2$ anomaly have revealed that Δa_μ can be totally contributed to by smuon-neutralino and sneutrino-chargino loops [96–98,103,111–162]. Since these contributions contain a chiral enhancement factor $\tan\beta$, the involved sleptons and electroweakinos may be sufficiently heavy to coincide with the LHC search for SUSY [162]. Joint interpretations of both anomalies were recently discussed in the Minimal Supersymmetric Standard Model (MSSM) [91,93,96,97,99]. It was found that even without the flavor violation, the theory could explain the anomalies at 1σ level by adjusting the magnitudes of the bino-slepton and chargino-sneutrino contributions for the electron and muon sectors [91]. The favored

parameter space was characterized by the selectrons and winolike electroweakinos lighter than about 200 GeV and the higgsinos heavier than about 1 TeV. These regions, however, have been excluded by the LHC search for SUSY according to our detailed Monte Carlo simulations [162]. Furthermore, given the general flavor structure of SUSY-breaking terms, the contribution of large nonuniversal trilinear A-terms could give the correct effect in principle [60,93,101]. Unfortunately, it seemed challenging to implement such anarchic A-terms with the SUSY-breaking mechanism while respecting all other flavor constraints [60]. These conclusions motivate us to conduct a more comprehensive study of the anomalies in the minimal realizations and explore as many possibilities of the theories as possible.

Notably, the direct detections of DM by the LUX-ZEPLIN (LZ) experiment [163] and the LHC search for SUSY [164–181] have required the higgsino mass in the MSSM to be significantly higher than the electroweak scale, namely, $\mu \gtrsim 500$ GeV, in explaining the muon $g-2$ anomaly at the 2σ level [162]. Although such a large μ may be generated by the well-known Giudice-Masiero mechanism in the gravity-mediated SUSY breaking scenario [182], it usually induces severe fine-tuning problems in the light of the LHC Higgs discovery and the absence of any SUSY discovery when the theory runs down from an infrared high energy scale to the electroweak scale [183–185]. Given the unnaturalness of the MSSM, we focus on the low energy Next-to-Minimal Supersymmetric Standard Model with a discrete $\mathbb{Z}_3$ symmetry ($\mathbb{Z}_3$-NMSSM), which is another economic realization of SUSY [186,187], to study the two anomalies. This model extends the MSSM with a singlet superfield $\hat{S}$ to dynamically generate the μ-parameter of the MSSM after the scalar component field of $\hat{S}$ develops a vacuum expectation value (vev) of $\mathcal{O}(1~{\rm TeV})$. Consequently, this theory is self-contained at the electroweak scale and owns much richer phenomenology than the MSSM as indicated by, e.g., Ref. [188–192]. As a preliminary study on this subject in the $\mathbb{Z}_3$-NMSSM, we assume no flavor violation in the lepton sector to simplify this work.

In our previous work [159], we investigated the impacts of the muon $g-2$ anomaly on the $\mathbb{Z}_3$-NMSSM by including the restrictions from the DM relic density [193], the direct detection of DM by the XENON-1T experiments [194,195], and the LHC search for SUSY [164–181]. We found that neither overly heavy supersymmetric particles nor moderately light sparticles were favored to explain the muon anomaly. In particular, we first obtained lower bounds on some SUSY parameters from those experimental restrictions, e.g., $|M_1| \gtrsim 275$ GeV, $M_2 \gtrsim 300$ GeV, $\mu \gtrsim 460$ GeV, $m_{\tilde{\mu}_L} \gtrsim 310$ GeV, and $m_{\tilde{\mu}_R} \gtrsim 350$ GeV, where M_1 and M_2 denoted the gaugino masses defined at the renormalization scale of 1 TeV and $m_{\tilde{\mu}_L}$ and $m_{\tilde{\mu}_R}$ were the masses of the muon-type sleptons

with L and R denoting their dominant chiral components, respectively. We also concluded by calculating the Bayesian evidence that the preferred DM candidate was the bino-dominated lightest neutralino rather than the singlino-dominated neutralino. It mainly coannihilated with the wino-dominated electroweakinos or the muon-type sleptons to obtain the measured density. In this work, we improve the previous study by freely varying the masses of the electron-type sleptons to predict a sizable $a_e^{\rm SUSY}$, which represents the SUSY contribution to a_e, and subsequently restricting the theory with the latest experimental results. We find that the LZ experiment and the LHC search for SUSY are complementary to each other in limiting the parameter space. The restrictions are so tight that they reduce $a_e^{\rm SUSY}$ from 3×10^{-13} to at most 1×10^{-13} when $a_\mu^{\rm SUSY}$ is fixed at 2.5×10^{-9}. We also find some subtleties about the results of the previous study after comparing them with those of this work.

This work is organized as follows. In Sec. II, we briefly recapitulated the dominant contributions to the lepton $g-2$ in the $\mathbb{Z}_3$-NMSSM and the status of the LHC search for SUSY. We studied the impacts of the leptonic anomalies on the $\mathbb{Z}_3$-NMSSM in Sec. III and compared them with those of Ref. [159], where we only considered the muon $g-2$ anomaly. After including relevant experimental constraints, we also presented the theory's electron and muon $g-2$ prediction. We summarized the conclusions in Sec. IV.

II. THEORETICAL PRELIMINARIES

A. Basics of the $\mathbb{Z}_3$-NMSSM

The $\mathbb{Z}_3$-NMSSM contains one extra singlet Higgs superfield $\hat{S}$ besides the usual two Higgs doublets, $\hat{H}_u$ and $\hat{H}_d$, of the MSSM. Consequently, the associated superpotential and soft SUSY breaking lagrangian of the $\mathbb{Z}_3$-NMSSM are given by [186,187]

$$W_{\rm NMSSM} = W_{\rm MSSM} + \lambda \hat{S} \hat{H}_u \cdot \hat{H}_d + \frac{1}{3}\kappa \hat{S}^3,$$

$$-\mathcal{L}_{\rm soft} = \left[A_\lambda \lambda S H_u \cdot H_d + \frac{1}{3}A_\kappa \kappa S^3 + {\rm H.c.} \right] \tag{2.1}$$

$$+ m_{H_u}^2 |H_u|^2 + m_{H_d}^2 |H_d|^2 + m_S^2 |S|^2 + \cdots. \tag{2.2}$$

The $W_{\rm MSSM}$ is the MSSM superpotential without the μ-term, λ and κ are dimensionless coefficients that parametrize the strength of Higgs self couplings, H_u, H_d, and S are the scalar parts of the superfields $\hat{H}_u$, $\hat{H}_d$, and $\hat{S}$, respectively, and the dimensional quantities $m_{H_u}^2$, $m_{H_d}^2$, m_S^2, A_λ, and A_κ are soft-breaking parameters. After the electroweak symmetry breaking, the fields H_u, H_d, and S acquire the vevs $v_u/\sqrt{2}$, $v_d/\sqrt{2}$, and $v_s/\sqrt{2}$, respectively, with $v \equiv \sqrt{v_u^2 + v_d^2} = 246$ GeV, and the interaction $\lambda \hat{S} \hat{H}_u \cdot \hat{H}_d$ generates an effective μ-term with $\mu = \lambda v_s/\sqrt{2}$. If the three vevs replace $m_{H_u}^2$, $m_{H_d}^2$, m_S^2 as theoretical inputs by the minimization conditions of the Higgs potential, the free parameters in the Higgs sector can be taken as follows [186]:

$$\lambda, \quad \kappa, \quad A_\lambda, \quad A_\kappa, \quad \mu, \quad \tan\beta \equiv v_u/v_d. \tag{2.3}$$

In the field convention that $H_{\rm SM} \equiv \sin\beta {\rm Re}(H_u^0) + \cos\beta {\rm Re}(H_d^0)$, $H_{\rm NSM} \equiv \cos\beta {\rm Re}(H_u^0) - \sin\beta {\rm Re}(H_d^0)$, and $A_{\rm NSM} \equiv \cos\beta {\rm Im}(H_u^0) - \sin\beta {\rm Im}(H_d^0)$, the elements of the CP-even Higgs boson mass matrix $\mathcal{M}_S^2$ in the bases $[H_{\rm NSM}, H_{\rm SM}, {\rm Re}(S)]$ are read as

$$M_{S,11}^2 = \frac{2\mu(A_\lambda + \kappa v_s)}{\sin 2\beta} + \frac{1}{2}(2m_Z^2 - \lambda^2 v^2)\sin^2 2\beta, \qquad M_{S,12}^2 = -\frac{1}{4}(2m_Z^2 - \lambda^2 v^2)\sin 4\beta,$$

$$M_{S,13}^2 = -\frac{1}{\sqrt{2}}(\lambda A_\lambda + 2\kappa\mu)v\cos 2\beta, \qquad M_{S,22}^2 = m_Z^2 \cos^2 2\beta + \frac{1}{2}\lambda^2 v^2 \sin^2 2\beta,$$

$$M_{S,23}^2 = \frac{v}{\sqrt{2}}[4\lambda\mu - (\lambda A_\lambda + 2\kappa\mu)\sin 2\beta],$$

$$M_{S,33}^2 = \frac{\lambda A_\lambda \sin 2\beta}{4\mu}\lambda v^2 + \kappa A_\kappa v_s + 4(\kappa v_s)^2 - \frac{1}{2}\lambda^2 v^2. \tag{2.4}$$

Then the mixings of the fields $H_{\rm NSM}$, $H_{\rm SM}$, and ${\rm Re}(S)$ result in three CP-even mass eigenstates denoted by h_i with $i = 1, 2, 3$ and satisfying $m_{h_1} < m_{h_2} < m_{h_3}$. Similarly, the mixing of $A_{\rm NSM}$ and ${\rm Im}(S)$ leads to two CP-odd states A_j with $j = 1, 2$ and satisfying $m_{A_1} < m_{A_2}$. The model also predicts a pair of charged Higgs bosons $H^\pm \equiv \cos\beta H_u^\pm + \sin\beta H_d^\pm$. In this study, the lightest CP-even Higgs boson h_1, instead of the next-lightest Higgs

boson h_2, is often treated as the LHC-discovered Higgs boson, denoted as h in this work, since the Bayesian evidence of the h_1-scenario is much larger than that of the h_2-scenario after considering the Higgs data collected at the LHC [159].

The electroweakino sector comprises bino ($\tilde{B}$), wino ($\tilde{W}$), higgsino ($\tilde{H}_u$ and $\tilde{H}_d$), and singlino ($\tilde{S}$) fields. Their mixings lead to five neutralinos $\tilde{\chi}_i^0$ with $i = 1, 2, ..., 5$,

arranged in ascending mass order, and two charginos $\tilde{\chi}_j^\pm$ with $j = 1,\ 2$ and satisfying $m_{\tilde{\chi}_1^\pm} < m_{\tilde{\chi}_2^\pm}$ [186]. Their masses and mixings are determined by the parameters M_1, M_2, λ, κ, $\tan\beta$, and μ, where the last four parameters also appear in the Higgs mass matrices.

B. Leptonic $g - 2$ in the $\mathbb{Z}_3$-NMSSM

The SUSY effects on the lepton anomalous magnetic moment a_ℓ ($\ell = e,\ \mu$) arise from the loops containing a chargino and a sneutrino and those mediated by a neutralino and a slepton [111,112]. The one-loop expressions of a_ℓ are [112]

$$a_\ell^{\rm SUSY} = a_\ell^{\tilde{\chi}^0\tilde{\ell}} + a_\ell^{\tilde{\chi}^\pm\tilde{\nu}},$$

$$a_\ell^{\tilde{\chi}^0\tilde{\ell}} = \frac{m_\ell}{16\pi^2}\sum_{i,k}\left\{-\frac{m_\ell}{12m_{\tilde{\ell}_k}^2}(|n_{ik}^{\rm L}|^2 + |n_{ik}^{\rm R}|^2)F_1^{\rm N}(x_{ik})\right.$$
$$\left. + \frac{m_{\tilde{\chi}_i^0}}{3m_{\tilde{\ell}_k}^2}{\rm Re}(n_{ik}^{\rm L}n_{ik}^{\rm R})F_2^{\rm N}(x_{ik})\right\},$$

$$a_\ell^{\tilde{\chi}^\pm\tilde{\nu}} = \frac{m_\ell}{16\pi^2}\sum_{j}\left\{\frac{m_\ell}{12m_{\tilde{\nu}_\ell}^2}(|c_j^{\rm L}|^2 + |c_j^{\rm R}|^2)F_1^{\rm C}(x_j)\right.$$
$$\left. + \frac{2m_{\tilde{\chi}_j^\pm}}{3m_{\tilde{\nu}_\ell}^2}{\rm Re}(c_j^{\rm L}c_j^{\rm R})F_2^{\rm C}(x_j)\right\},$$

where $i = 1, ..., 5$, $j = 1,\ 2$, and $k = 1,\ 2$ refer to the neutralino, chargino, and slepton indices, respectively. The involved couplings are given by

$$n_{ik}^{\rm L} = \frac{1}{\sqrt{2}}(g_2 N_{i2} + g_1 N_{i1})X_{k1}^{\ell,*} - Y_\ell N_{i3}X_{k2}^{\ell,*}, \quad c_j^{\rm L} = -g_2 V_{j1},$$
$$n_{ik}^{\rm R} = \sqrt{2}g_1 N_{i1}X_{k2}^\ell + Y_\ell N_{i3}X_{k1}^\ell, \quad c_j^{\rm R} = Y_\ell U_{j2}, \tag{2.5}$$

where N, X, and U and V are the rotation matrices of the neutralinos, the sleptons, and the charginos, respectively [186]. The kinematic loop functions $F_i(x)$ take the following forms:

$$F_1^{\rm N}(x) = \frac{2}{(1-x)^4}(1 - 6x + 3x^2 + 2x^3 - 6x^2\ln x),$$
$$F_2^{\rm N}(x) = \frac{3}{(1-x)^3}(1 - x^2 + 2x\ln x),$$
$$F_1^{\rm C}(x) = \frac{2}{(1-x)^4}(2 + 3x - 6x^2 + x^3 + 6x\ln x),$$
$$F_2^{\rm C}(x) = -\frac{3}{2(1-x)^3}(3 - 4x + x^2 + 2\ln x), \tag{2.6}$$

with $x_{ik} \equiv m_{\tilde{\chi}_i^0}^2/m_{\tilde{\ell}_k}^2$ and $x_j \equiv m_{\tilde{\chi}_j^\pm}^2/m_{\tilde{\nu}_\ell}^2$, and they satisfy $F_i(1) = 1$.

It is instructive to understand the behavior of $a_\ell^{\rm SUSY}$ by the mass insertion approximation [113]. In this method, the

SUSY contributions to a_ℓ are classified into four types: "WHL", "BHL", "BHR," and "BLR," where W, B, H, L, and R stand for wino, bino, higgsino, left-handed slepton or sneutrino, and right-handed slepton fields, respectively. They arise from the Feynman diagrams involving $\tilde{W} - \tilde{H}_d$, $\tilde{B} - \tilde{H}_d^0$, $\tilde{B} - \tilde{H}_d^0$, and $\tilde{\ell}_L - \tilde{\ell}_R$ transitions, respectively, and have the following form [113,115,116]:

$$a_{\ell,{\rm WHL}}^{\rm SUSY} = \frac{\alpha_2}{8\pi}\frac{m_\ell^2 M_2\mu\tan\beta}{M_{\tilde{\nu}_\ell}^4}$$
$$\times\left\{2f_C\left(\frac{M_2^2}{M_{\tilde{\nu}_\ell}^2}, \frac{\mu^2}{M_{\tilde{\nu}_\ell}^2}\right) - \frac{M_{\tilde{\nu}_\ell}^4}{M_{\tilde{\ell}_L}^4}f_N\left(\frac{M_2^2}{M_{\tilde{\ell}_L}^2}, \frac{\mu^2}{M_{\tilde{\ell}_L}^2}\right)\right\}, \tag{2.7}$$

$$a_{\ell,{\rm BHL}}^{\rm SUSY} = \frac{\alpha_Y}{8\pi}\frac{m_\ell^2 M_1\mu\tan\beta}{M_{\tilde{\ell}_L}^4}f_N\left(\frac{M_1^2}{M_{\tilde{\ell}_L}^2}, \frac{\mu^2}{M_{\tilde{\ell}_L}^2}\right), \tag{2.8}$$

$$a_{\ell,{\rm BHR}}^{\rm SUSY} = -\frac{\alpha_Y}{4\pi}\frac{m_\ell^2 M_1\mu\tan\beta}{M_{\tilde{\ell}_R}^4}f_N\left(\frac{M_1^2}{M_{\tilde{\ell}_R}^2}, \frac{\mu^2}{M_{\tilde{\ell}_R}^2}\right), \tag{2.9}$$

$$a_{\ell,{\rm BLR}}^{\rm SUSY} = \frac{\alpha_Y}{4\pi}\frac{m_\ell^2 M_1\mu\tan\beta}{M_1^4}f_N\left(\frac{M_{\tilde{\ell}_L}^2}{M_1^2}, \frac{M_{\tilde{\ell}_R}^2}{M_1^2}\right), \tag{2.10}$$

where $M_{\tilde{\ell}_L}$ and $M_{\tilde{\ell}_R}$ are soft-breaking masses for the left-handed and right-handed slepton fields, respectively, at the slepton mass scale, and they are approximately equal to the slepton masses. The loop functions are given by

$$f_C(x,y) = \frac{5 - 3(x+y) + xy}{(x-1)^2(y-1)^2} - \frac{2\ln x}{(x-y)(x-1)^3}$$
$$+ \frac{2\ln y}{(x-y)(y-1)^3}, \tag{2.11}$$

$$f_N(x,y) = \frac{-3 + x + y + xy}{(x-1)^2(y-1)^2} + \frac{2x\ln x}{(x-y)(x-1)^3}$$
$$- \frac{2y\ln y}{(x-y)(y-1)^3}, \tag{2.12}$$

and they have the property that $f_C(1,1) = 1/2$ and $f_N(1,1) = 1/6$.

The following properties of $a_\ell^{\rm SUSY}$ should be noted:

(i) If all the dimensional SUSY parameters involved in $a_\ell^{\rm SUSY}$ take a common value $M_{\rm SUSY}$, $a_\ell^{\rm SUSY}$ is proportional to $m_\ell^2\tan\beta/M_{\rm SUSY}^2$. In this case, $a_e^{\rm SUSY}$ and $a_\mu^{\rm SUSY}$ are correlated by $a_\mu^{\rm SUSY}/a_e^{\rm SUSY} = m_\mu^2/m_e^2$, and $a_\mu^{\rm SUSY} = (25.1, 25.1 - 5.9, 25.1 - 2 \times 5.9) \times 10^{-10}$ corresponds to $a_e^{\rm SUSY} = (5.85, 4.47, 3.10) \times 10^{-14}$, respectively. This conclusion reflects that the electron $g - 2$ anomaly prefers a much lower SUSY scale than the muon $g - 2$ anomaly.

(ii) The "WHL" contribution in each a_ℓ^{SUSY} is usually much larger than the other contributions if $\tilde{\ell}_L$ is not significantly heavier than $\tilde{\ell}_R$ [146].

(iii) The four types of contributions have different dependence on the parameter μ. Specifically, $a_{\ell,\mathrm{BLR}}^{\mathrm{SUSY}}$ is proportional to the higgsino mass μ, while the others contain both a preactor of μ and a loop function that tends to be zero as μ approaches infinity. We observe that the "WHL" contribution monotonically decreases with increasing μ for several typical cases of particle mass spectra. By contrast, the "BHL" and "BHR" contributions increase when μ is significantly smaller than the slepton masses and decrease if μ is larger than the slepton masses.

(iv) Since the singlino field appears in the "WHL," "BHL," and "BHR" loops by two-time insertions, its contribution to a_ℓ^{SUSY} is never prominent, considering $\lambda \lesssim 0.3$ for most cases in this study. Therefore, a_ℓ^{SUSY} in the $\mathbb{Z}_3$-NMSSM is almost equal to that in the MSSM.

(v) The difference of a_ℓ^{SUSY} calculated by the mass insertion approximation and the full expression, respectively, is less than 3%. We verified this point by studying the samples acquired by the following parameter scan.

(vi) The two-loop (2L) contributions to a_ℓ^{SUSY}, including 2L corrections to the SM one-loop diagrams and those to the SUSY one-loop diagrams [117], are

about -5% of the one-loop prediction [161]. They were neglected in this study.

C. LHC search for SUSY

To explain the electron and muon $g-2$ anomalies in the $\mathbb{Z}_3$-NMSSM simultaneously, both the electroweakinos and the first two-generation sleptons must be moderately light. The LHC experiments have strongly limited such a situation by searching for the multilepton plus missing momentum signal. We present pertinent experimental analyses in Tables I and II. Notably, the following ones play a crucial role in restricting the situation:

(i) `CMS-SUS-20-001` [166]: Search for the SUSY signal containing two oppositely charged same-flavor leptons and missing transverse momentum. This analysis investigated not only the squark and gluino productions but also the electroweakino and slepton productions. The lepton arose from an on-shell or off-shell Z boson in the decay chain or from the direct decay of the produced sleptons. The wino-dominated chargino and neutralino were explored up to 750 GeV and 800 GeV, respectively, in mass by the electroweakino pair production processes, while the first two-generation sleptons were explored up to a mass of 700 GeV by the slepton pair production processes, assuming the sleptons were degenerate in mass.

TABLE I. Experimental analyses of the electroweakino production processes at the 13 TeV LHC, categorized by the topologies of the SUSY signals. They were utilized to limit the parameter points of this study.

Scenario	Final State	Name
$\tilde{\chi}_2^0 \tilde{\chi}_1^\pm \to WZ\tilde{\chi}_1^0\tilde{\chi}_1^0$	$n\ell(n \geq 2) + nj(n \geq 0) + E_T^{\mathrm{miss}}$	CMS-SUS-20-001 (137 fb^{-1}) [166]
		ATLAS-2106-01676 139 fb^{-1} [165]
		CMS-SUS-17-004 (35.9 fb^{-1}) [167]
		CMS-SUS-16-039 (35.9 fb^{-1}) [168]
		ATLAS-1803-02762 (36.1 fb^{-1}) [169]
		ATLAS-1806-02293 (36.1 fb^{-1}) [170]
$\tilde{\chi}_2^0 \tilde{\chi}_1^\pm \to \ell\tilde{\nu}\ell\tilde{\ell}$	$n\ell(n = 3) + E_T^{\mathrm{miss}}$	CMS-SUS-16-039 (35.9 fb^{-1}) [168]
		ATLAS-1803-02762 (36.1 fb^{-1}) [169]
$\tilde{\chi}_2^0 \tilde{\chi}_1^\pm \to \tilde{\tau}\nu\ell\tilde{\ell}$	$2\ell + 1\tau + E_T^{\mathrm{miss}}$	CMS-SUS-16-039 (35.9 fb^{-1}) [168]
$\tilde{\chi}_2^0 \tilde{\chi}_1^\pm \to \tilde{\tau}\nu\tilde{\tau}\tau$	$3\tau + E_T^{\mathrm{miss}}$	CMS-SUS-16-039 (35.9 fb^{-1}) [168]
$\tilde{\chi}_2^0 \tilde{\chi}_1^\pm \to Wh\tilde{\chi}_1^0\tilde{\chi}_1^0$	$n\ell(n \geq 1) + nb(n \geq 0) + nj(n \geq 0) + E_T^{\mathrm{miss}}$	ATLAS-1909-09226 (139 fb^{-1}) [171]
		CMS-SUS-17-004 (35.9 fb^{-1}) [167]
		CMS-SUS-16-039 (35.9 fb^{-1})[168]
		ATLAS-1812-09432 (36.1 fb^{-1}) [172]
		CMS-SUS-16-034 (35.9 fb^{-1}) [173]
		CMS-SUS-16-045 (35.9 fb^{-1}) [174]
$\tilde{\chi}_1^\mp \tilde{\chi}_1^\pm \to WW\tilde{\chi}_1^0\tilde{\chi}_1^0$	$2\ell + E_T^{\mathrm{miss}}$	ATLAS-1908-08215 (139 fb^{-1}) [164]
		CMS-SUS-17-010 (35.9 fb^{-1}) [175]

(Table continued)

TABLE I. *(Continued)*

Scenario	Final State	Name
$\tilde{\chi}_1^{\mp}\tilde{\chi}_1^{\pm} \to 2\tilde{\ell}\nu(\tilde{\nu}\ell)$	$2\ell + E_T^{miss}$	ATLAS-1908-08215 (139 fb^{-1}) [164]
		CMS-SUS-17-010 (35.9 fb^{-1}) [175]
$\tilde{\chi}_2^0\tilde{\chi}_1^{\mp} \to h/ZW\tilde{\chi}_1^0\tilde{\chi}_1^0, \tilde{\chi}_1^0 \to \gamma/Z\tilde{G}$	$2\gamma + n\ell(n \geq 0) + nb(n \geq 0) + nj(n \geq 0) + E_T^{miss}$	ATLAS-1802-03158 (36.1 fb^{-1}) [176]
$\tilde{\chi}_1^{\pm}\tilde{\chi}_1^{\mp} \to WW\tilde{\chi}_1^0\tilde{\chi}_1^0, \tilde{\chi}_1^0 \to \gamma/Z\tilde{G}$		
$\tilde{\chi}_2^0\tilde{\chi}_1^{\pm} \to ZW\tilde{\chi}_1^0\tilde{\chi}_1^0, \tilde{\chi}_1^0 \to h/Z\tilde{G}$	$n\ell(n \geq 4) + E_T^{miss}$	ATLAS-2103-11684 (139 fb^{-1}) [177]
$\tilde{\chi}_1^{\pm}\tilde{\chi}_1^{\mp} \to WW\tilde{\chi}_1^0\tilde{\chi}_1^0, \tilde{\chi}_1^0 \to h/Z\tilde{G}$		
$\tilde{\chi}_2^0\tilde{\chi}_1^0 \to Z\tilde{\chi}_1^0\tilde{\chi}_1^0, \tilde{\chi}_1^0 \to h/Z\tilde{G}$		
$\tilde{\chi}_1^{\mp}\tilde{\chi}_1^0 \to W\tilde{\chi}_1^0\tilde{\chi}_1^0, \tilde{\chi}_1^0 \to h/Z\tilde{G}$		
$\tilde{\chi}_i^{0,\pm}\tilde{\chi}_j^{0,\mp} \to \tilde{\chi}_1^0\tilde{\chi}_1^0 + \chi_{soft} \to ZZ/H\tilde{G}\tilde{G}$	$n\ell(n \geq 2) + nb(n \geq 0) + nj(n \geq 0) + E_T^{miss}$	CMS-SUS-16-039 (35.9 fb^{-1}) [168]
		CMS-SUS-17-004 (35.9 fb^{-1}) [167]
		CMS-SUS-20-001 (137 fb^{-1}) [166]
$\tilde{\chi}_i^{0,\pm}\tilde{\chi}_j^{0,\mp} \to \tilde{\chi}_1^0\tilde{\chi}_1^0 + \chi_{soft} \to HH\tilde{G}\tilde{G}$	$n\ell(n \geq 2) + nb(n \geq 0) + nj(n \geq 0) + E_T^{miss}$	CMS-SUS-16-039 (35.9 fb^{-1}) [168]
		CMS-SUS-17-004 (35.9 fb^{-1}) [167]
$\tilde{\chi}_2^0\tilde{\chi}_1^{\pm} \to W^*Z^*\tilde{\chi}_1^0\tilde{\chi}_1^0$	$3\ell + E_T^{miss}$	ATLAS-2106-01676 (139 fb^{-1}) [165]
$\tilde{\chi}_2^0\tilde{\chi}_1^{\pm} \to Z^*W^*\tilde{\chi}_1^0\tilde{\chi}_1^0$	$2\ell + nj(n \geq 0) + E_T^{miss}$	ATLAS-1911-12606 (139 fb^{-1}) [178]
		ATLAS-1712-08119 (36.1 fb^{-1}) [179]
		CMS-SUS-16-048 (35.9 fb^{-1}) [180]
$\tilde{\chi}_2^0\tilde{\chi}_1^{\pm} + \tilde{\chi}_1^{\pm}\tilde{\chi}_1^{\mp} + \tilde{\chi}_1^{\pm}\tilde{\chi}_1^0$	$2\ell + nj(n \geq 0) + E_T^{miss}$	ATLAS-1911-12606 (139 fb^{-1}) [178]
		ATLAS-1712-08119 (36.1 fb^{-1}) [179]
		CMS-SUS-16-048 (35.9 fb^{-1}) [180]

(ii) `CMS-SUS-16-039` and `CMS-SUS-17-004` [167,168]: Search for the electro-weakino productions by the final state containing two, three, or four leptons and missing transverse momentum (E_T^{miss}). The analyses included all possible final states and defined several categories by the number of leptons in the event, their flavor and charges to improve the discovery potential. In the context of the simplified model of SUSY, the observed limit on the wino-dominated $m_{\tilde{\chi}_1^{\pm}}$ in the chargino-neutralino production was 650 GeV for the WZ topology, 480 GeV for the WH topology, and 535 GeV for the mixed topology. Remarkably, these analyses studied only 35.9 fb^{-1} data collected at the Run-II phase of the LHC.

(iii) `ATLAS-2106-01676` [165]: Search for the signals of the wino- and higgsino-dominated chargino-neutralino associated productions. It investigated on-shell WZ, off-shell WZ, and Wh categories in the decay chain and concentrated on the final state containing exactly three leptons, possible ISR jets, and E_T^{miss}. The exclusion bound of $m_{\tilde{\chi}_2^0}$ was 640 GeV for a massless $\tilde{\chi}_1^0$ in the wino scenario of the simplified model. It was weakened as the mass difference between $\tilde{\chi}_2^0$ and $\tilde{\chi}_1^0$ reduced. Specifically, $\tilde{\chi}_2^0$ should be heavier than 500 GeV for $m_{\tilde{\chi}_1^0} = 300$ GeV (the on-shell W/Z case), 300 GeV for a positive $m_{\tilde{\chi}_1^0}$ and 35 GeV $\lesssim m_{\tilde{\chi}_2^0} - m_{\tilde{\chi}_1^0} \lesssim 90$ GeV (the off-shell W/Z case), and 220 GeV when $m_{\tilde{\chi}_1^0}$ is positive and $m_{\tilde{\chi}_2^0} - m_{\tilde{\chi}_1^0} = 15$ GeV (the extreme off-shell W/Z case). By contrast, $\tilde{\chi}_2^0$ was excluded only up to a mass of 210 GeV in the off-shell W/Z case of the higgsino scenario, occurring when $m_{\tilde{\chi}_2^0} - m_{\tilde{\chi}_1^0} = 10$ GeV or $m_{\tilde{\chi}_2^0} - m_{\tilde{\chi}_1^0} \gtrsim 35$ GeV.

TABLE II. Same as Table I, but for the slepton production processes.

Scenario	Final State	Name
$\tilde{\ell}\tilde{\ell} \to \ell\ell\tilde{\chi}_1^0\tilde{\chi}_1^0$	$2\ell + E_T^{miss}$	ATLAS-1911-12606 (139 fb^{-1}) [178]
		ATLAS-1712-08119 (36.1 fb^{-1})[179]
		ATLAS-1908-08215 (139 fb^{-1})[164]
		CMS-SUS-20-001 (137 fb^{-1}) [166]
		ATLAS-1803-02762 (36.1 fb^{-1})[169]
		CMS-SUS-17-009 (35.9 fb^{-1})[181]

(iv) `ATLAS-1911-12606` [178]: Search for the electroweakino pair productions and the slepton pair productions by two leptons and missing transverse momentum in the final state. This analysis concentrated on the scenario of compressed mass spectra and projected its results onto $\Delta m - \tilde{\chi}_2^0$ plane, where $\Delta m \equiv m_{\tilde{\chi}_2^0} - m_{\tilde{\chi}_1^0}$ for the electroweakino production. It was found that the tightest bounds on the higgsino- and wino-dominated $\tilde{\chi}_2^0$ were 193 GeV in mass for $\Delta m \simeq 9.3$ GeV and 240 GeV in mass for $\Delta m \simeq 7$ GeV, respectively. Similar lower mass limit on degenerate light-flavor sleptons was 250 GeV for $\Delta m_{\tilde{\ell}} \equiv m_{\tilde{\ell}} - m_{\tilde{\chi}_1^0} = 10$ GeV.

III. NUMERICAL RESULTS

This work used the package SARAH 4.14.3 [196–199] to build the model file of the $\mathbb{Z}_3$-NMSSM, the codes SPHENO 4.0.4 [200,201] and FLAVORKIT [202] to generate particle mass spectra and calculate low energy observables such as a_ℓ^{SUSY} and B-physics measurements, and the package MicrOMEGAs 5.0.4 [203–208] to compute DM observables, assuming the lightest neutralino as the sole DM candidate in the universe. Bounds from the direct search for extra Higgs bosons at LEP, Tevatron, and LHC and the fit of Higgs property to pertinent experimental data were implemented by the codes HiggsBounds 5.3.2 [209–212] and HiggsSignal 2.2.3 [213–216], respectively.

A. Research strategy

In our previous work [159], we performed two independent scans of the parameter space in the $\mathbb{Z}_3$-NMSSM to reveal the salient features of a_μ^{SUSY}, using the MultiNest algorithm [217] with the setting $n_{\mathrm{live}} = 8000$. In the first one, we fixed $A_\lambda = 2$ TeV and varied the parameters in the

sectors of muon-type sleptons, electroweakinos, and Higgs bosons. The second scan was similar to the first one, except that we also varied A_λ. The results of these scans were identical in many aspects, indicating that the involved physics was insensitive to A_λ or, equivalently, the mass of the heavy doublet Higgs bosons, m_A, defined by $m_A^2 \equiv 2\mu(A_\lambda + 2\kappa v_s)/\sin 2\beta$. This study updated the first scan by varying the parameters in both the electron- and muon-type slepton sectors since we would explore the combined effects of Δa_μ and Δa_e on the theory. We presented the details of the surveyed parameter space in Table III, and correspondingly, used the following likelihood function to guide the scan,

$$
\begin{aligned}
\mathcal{L} &= \mathcal{L}_{\mathrm{Res}} \times \mathcal{L}_{a_\mu^{\mathrm{SUSY}}} \times \mathcal{L}_{a_e^{\mathrm{SUSY}}} \\
&= \mathcal{L}_{\mathrm{Res}} \times \exp\Bigg\{ -\frac{1}{2}\Bigg[\left(\frac{a_\mu^{\mathrm{SUSY}} - 2.51 \times 10^{-9}}{5.9 \times 10^{-10}} \right)^2 \\
&\quad + \left(\frac{a_e^{\mathrm{SUSY}} - 4.8 \times 10^{-13}}{3.0 \times 10^{-13}} \right)^2 \Bigg] \Bigg\},
\end{aligned}
$$

where $\mathcal{L}_{\mathrm{Res}}$ represented the restrictions of pertinent experiments on the theory: $\mathcal{L}_{\mathrm{Res}} = 1$ by our definition if the limitations are satisfied, and otherwise, $\mathcal{L}_{\mathrm{Res}} = \mathrm{Exp}[-100]$. These limitations include:

(i) DM relic density, $0.096 < \Omega h^2 < 0.144$. We took the central value of $\Omega h^2 = 0.120$ from the Planck-2018 data [193] and assumed a theoretical uncertainty of 20% in the density calculation.

(ii) DM direct detection bound from the XENON-1T experiments [194,195] on both the spin-independent (SI) DM-nucleon scattering cross-section, σ_p^{SI}, and the spin-dependent (SD) neutron-nucleon cross-section, σ_n^{SD}. The DM indirect detections from the observation of dwarf galaxies by the Fermi-LAT collaboration were not included since they had no restrictions on the theory when $|m_{\tilde{\chi}_1^0}| \gtrsim 100$ GeV [218].

(iii) Higgs data fit. Given that one of the CP-even Higgs bosons corresponded to the LHC-discovered Higgs boson, its properties should coincide with the Higgs measurements by ATLAS and CMS collaborations at the 95% confidence level. A p-value larger than 0.05 is essential, which was tested by the code HiggsSignal 2.2.3 [213–216].

(iv) Direct search for extra Higgs bosons at LEP, Tevatron and LHC. This requirement was examined by the code HiggsBounds 5.3.2 [209–212].

(v) B-physics measurements. The branching ratios of $B_s \to \mu^+\mu^-$ and $B \to X_s\gamma$ should be consistent with their experimental measurements at the 2σ level [219].

(vi) Vacuum stability. The vacuum state of the scalar potential comprising the Higgs fields and the first two-generation slepton fields should be either stable

TABLE III. The parameter space explored in this study, where $M_{\tilde{\ell}_L}$ and $M_{\tilde{\ell}_R}$ with $\ell = e, \mu$ denote the soft-breaking mass of the left- and right-handed slepton fields, respectively. The soft trilinear coefficients for the third-generation squarks, represented by A_t and A_b, were assumed equal. The gluino mass was fixed at $M_3 = 3$ TeV. The other dimensional SUSY parameters were not crucial, and they took a shared value of 2 TeV in this study, including A_λ and the unmentioned soft-breaking parameters in the squark and slepton sectors. All the input parameters were defined at the renormalization scale $Q = 1$ TeV.

Parameter	Prior	Range	Parameter	Prior	Range
λ	Flat	0.01–0.7	κ	Flat	−0.7–0.7
$\tan\beta$	Flat	1.0–60.0	$A_t/$TeV	Flat	−5.0–5.0
$\mu/$TeV	Log	0.1–1.0	$A_\kappa/$TeV	Flat	−1.0–1.0
$M_1/$TeV	Flat	−1.5 ∼ 1.5	$M_2/$TeV	Log	0.1–1.5
$M_{\tilde{\mu}_L}/$TeV	Log	0.1–1.0	$M_{\tilde{\mu}_R}/$TeV	Log	0.1–1.0
$M_{\tilde{e}_L}/$TeV	Log	0.1–1.0	$M_{\tilde{e}_R}/$TeV	Log	0.1–1.0

or long-lived. This condition was tested by the code VEVACIOUS [220].

In the following, we were particularly interested in the samples obtained by the scan that predicted $a_e^{\text{SUSY}} > 0$, explained the muon $g - 2$ anomaly at the 2σ level, and meanwhile, coincided with all the restrictions. We decided whether they pass the restrictions from the LHC search for SUSY in Tables I and II by simulating the following processes with the Monte Carlo (MC) method:

$$
\begin{aligned}
pp &\to \tilde{\chi}_i^0 \tilde{\chi}_j^\pm, && i = 2, 3, 4, 5; && j = 1, 2 \\
pp &\to \tilde{\chi}_i^\pm \tilde{\chi}_j^\mp, i, && j = 1, 2; \\
pp &\to \tilde{\chi}_i^0 \tilde{\chi}_j^0, i, && j = 2, 3, 4, 5; \\
pp &\to \tilde{\ell}_i^* \tilde{\ell}_j, && i, j = L, R; && pp \to \tilde{\nu}_\ell^* \tilde{\nu}_\ell. \quad (3.1)
\end{aligned}
$$

Specifically, we calculated their cross-sections at $\sqrt{s} = 13$ TeV by the package PROSPINO2 [221] to the next-to-leading order. To save computation time, we initially used the program SMODELS 2.1.1, which encoded various event-selection efficiencies by the topologies of SUSY signals [222], to exclude these samples. Given that this program's capability to implement the LHC restrictions was limited by its database and strict working prerequisites, we further surveyed the remaining samples by simulating the analyses in Tables I and II. We accomplished this task by following steps: we first generated 60000 and 40000 events for the electroweakino and slepton production processes, respectively, by the package MadGraph_aMC@NLO [223,224], then finished the parton shower and hadronization by the program PYTHIA8 [225], and finally fed the resulting event files into the package CHECKMATE 2.0.29 [226–228], which incorporated the program DELPHES for detector simulation [229], to calculate the R-value defined by $R \equiv \max\{S_i/S_{i,\text{obs}}^{95}\}$ (S_i denotes the simulated event number of the ith SR in the analyses of Tables I and II, and $S_{i,\text{obs}}^{95}$ represents its corresponding 95% confidence level upper limit). Evidently, without considering the involved experimental and theoretical uncertainties, $R > 1$ implied that the studied parameter point was excluded due to its inconsistency with the LHC results [230]. Otherwise, it was experimentally allowed.

We emphasize that this study is a continuation of Ref. [159], which included the XENON-1T restrictions and only studied the influence of the muon $g - 2$ anomaly on the $\mathbb{Z}_3$-NMSSM. We first used the XENON-1T results instead of the latest LZ results to limit the parameter space of the theory in Sec. III B. The purpose was to clarify the impacts of the electron anomaly alone by comparing this study's results with those of Ref. [159]. Subsequently, we focused on the subset of the samples which further satisfy the LZ limits. We performed an analogous analysis in Sec. III C, i.e., we compared the acquired conclusions with those obtained from the samples surviving the XENON-1T

limits to illustrate the effects of the LZ experiment. These operations allowed us to separately investigate the influences of the electron $g - 2$ anomaly, the LZ experiment, and the LHC search for SUSY on the $\mathbb{Z}_3$-NMSSM and presented their features in order. It is beneficial to demonstrate the underlying physics.

B. Impacts of Δa_e on the $\mathbb{Z}_3$-NMSSM

As we introduced before, the research strategy of this study is the same as that of our previous work on the muon $g - 2$ anomaly in Ref. [159], except that we additionally included the electron $g - 2$ anomaly in the likelihood function and correspondingly, we varied the parameters $M_{\tilde{e}_L}$ and $M_{\tilde{e}_R}$. Consequently, the two studies share many features in their results, which are summarized as follows:

(i) The DM candidate and the LHC-discovered Higgs boson are identified as the bino-dominated lightest neutralino and the lightest CP-even Higgs boson, respectively, in most cases. The Bayesian evidence of different scenarios testified to this conclusion [159].

(ii) The DM candidate $\tilde{\chi}_1^0$ achieves the measured relic density by co-annihilating with the winolike electroweakinos or the sleptons. Because the electroweakinos comprise two particles, namely $\tilde{\chi}_2^0$ and $\tilde{\chi}_1^\pm$, with approximately degenerate masses, and both of them have stronger interactions with the SM particles in comparison with the sleptons, the former mechanism can acquire the measured density by broader mass splittings between $\tilde{\chi}_1^0$ and its coannihilation partners than the latter annihilation [231]. As a result, the former mechanism more readily works [159]. By contrast, the Z and Higgs resonant annihilations are disfavored experimentally and theoretically in obtaining the density [162]. We will discuss this issue later.

(iii) Since a negative μM_1 can suppress the DM-nucleon SI scattering cross-section by canceling different contributions, most samples yielded by the scan predict $M_1 < 0$ [159]. In addition, the XENON-1T experiments alone require $\mu \gtrsim 300$ GeV, given the measured density [162].

(iv) $\tilde{\chi}_1^0$ must be lighter than 620 GeV to explain the $(g - 2)_\mu$ anomaly at the 2σ level. With the increase of $|m_{\tilde{\chi}_1^0}|$, the maximum reach of μ, $m_{\tilde{\mu}_L}$, and $m_{\tilde{\mu}_R}$ decreases monotonously. This trend is more significant for μ and $m_{\tilde{\mu}_L}$ than for $m_{\tilde{\mu}_R}$ [159]. The fundamental reason comes from the facts that the $\mathbb{Z}_3$-NMSSM is a decoupled theory in the heavy sparticle limit and a_μ^{SUSY} is more sensitive to μ and $m_{\tilde{\mu}_L}$ than to $m_{\tilde{\mu}_R}$. $m_{\tilde{e}_L}$ and $m_{\tilde{e}_R}$ show similar behaviors when fixing a_e^{SUSY} at a positively sizable value.

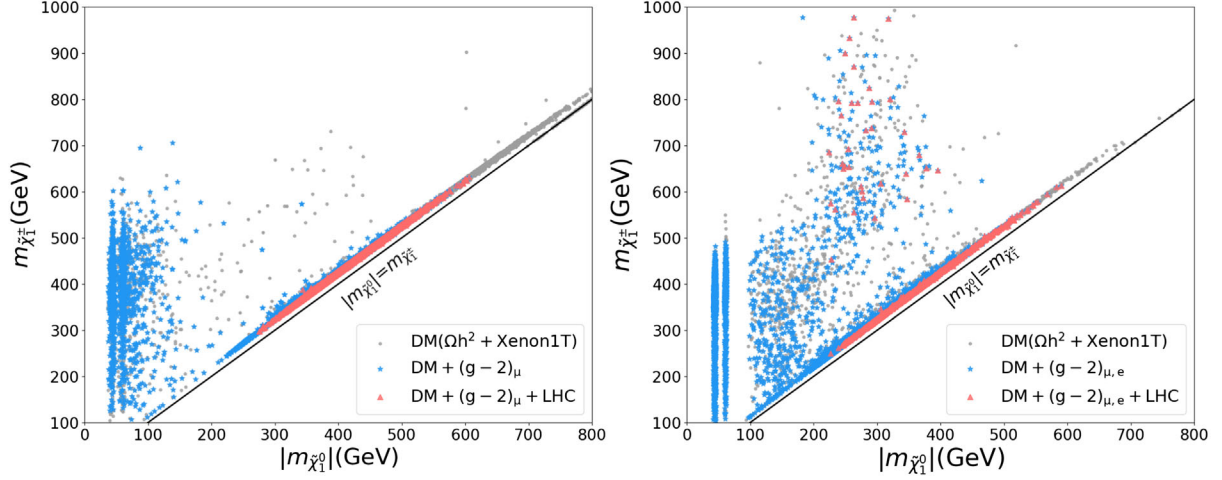(v) Since explaining the muon $g - 2$ anomaly needs more than one sparticle to be moderately light, the

FIG. 1. Projection of the samples yielded by the first scan of Ref. [159] and the scan of this work onto the $|m_{\tilde{\chi}_1^0}| - m_{\tilde{\chi}_1^\pm}$ planes, which are shown in the left and right panels, respectively. The gray dots denote the samples that survive all the restrictions listed in the text, in particular those from the DM experiments. The blue stars represent the parameter points that further explain the muon $g - 2$ anomaly at the 2σ level. They also predict $a_e^{\mathrm{SUSY}} > 0$ in the right panel. The red triangles are part of the blue stars which coincide with the results of the LHC search for SUSY. Note that the left panel only considered the impacts of the muon $g - 2$ anomaly on the $\mathbb{Z}_3$-NMSSM, which was realized in the scan of Ref. [159] by varying $M_{\tilde{\mu}_L}$ and $M_{\tilde{\mu}_R}$ while fixing $M_{\tilde{e}_L} = M_{\tilde{e}_R} = 1$ TeV. By contrast, the right panel demonstrated the combined effects of the muon and electron $g - 2$ anomalies on the theory, as described by the research strategy in Sec. III A. Although the left panel has been studied in Ref. [159], we provide it here to make the differences induced by adding the electron anomaly into the likelihood function distinct and deepen the researcher's impression of the effects of the electron anomaly.

restrictions from the LHC search for SUSY on the $\mathbb{Z}_3$-NMSSM are tight. As a result, the involved sparticles must be relatively heavy to coincide with the experimental results, e.g., $|m_{\tilde{\chi}_1^0}| \gtrsim 275$ GeV, $m_{\tilde{\chi}_1^\pm} \gtrsim 300$ GeV, and $m_{\tilde{\mu}_L} \gtrsim 310$ GeV, as obtained in Ref. [159]. The primary reasons are as follows: if $\tilde{\chi}_1^0$ is lighter, more missing momentum will be emitted in the sparticle production processes at the LHC, which can improve the sensitivities of the experimental analyses; if the sparticles other than $\tilde{\chi}_1^0$ are lighter, they will be copiously produced at the LHC to increase the events containing the multiple leptons.

In addition, there are two cases that the LHC restrictions are extreme [159,162]. One is characterized by $\tan\beta \lesssim 20$, where winos, higgsinos, and left-handed dominant smuon are all lighter than 500 GeV to explain the muon $g - 2$ anomaly at the 2σ level. The other is characterized by predicting a $\tilde{\mu}_L$ lighter than winos and/or higgsinos, where the heavy electroweakinos may decay into $\tilde{\mu}_L$ first and thus enhance the leptonic signal of the electroweakino pair production processes (compared with the very massive $\tilde{\mu}_L$ case).

We found that the signal regions of more than three leptons in CMS-SUS-16-039 and more than 200 GeV of E_T^{miss} in CMS-SUS-20-001 played a crucial role in excluding the parameter space [159]. We presented more details of the LHC restrictions in Ref. [162].

(vi) As required by the Higgs data fit, all the samples yielded by the scans predicted $\lambda \lesssim 0.3$. Consequently, the involved physics of the $\mathbb{Z}_3$-NMSSM

is approximately the same as that of the MSSM. This conclusion was recently testified to by an elaborate study of the MSSM in Ref. [162].

(vii) Since some of the involved sparticles cannot be hefty, e.g., $\tilde{\chi}_1^0$ and $\tilde{\chi}_1^\pm$ should be lighter than 700 GeV, future colliders, such as the International Linear Collider with $\sqrt{s} = 1$ TeV [232], can explore different SUSY explanations of the anomalies [233].

Despite these similarities, there are two significant differences of the results, which include

(i) The posterior distributions of the samples yielded by the scans. To illustrate this point, we projected the SUSY parameter points acquired in the first scan of Ref. [159] and those caught in this study onto the $|m_{\tilde{\chi}_1^0}| - m_{\tilde{\chi}_1^\pm}$ planes to obtain the left and right panels of Fig. 1, respectively. The left panel indicates that nearly all the samples predicting $|m_{\tilde{\chi}_1^0}| \gtrsim 250$ GeV acquire the measured density by coannihilating with the winolike electroweakinos. By contrast, the right panel shows that a sizable portion of such points can achieve the measured density by coannihilating with either the electron-type or muon-type sleptons. In addition, only sparse samples predict 100 GeV $\leq |m_{\tilde{\chi}_1^0}| \leq 250$ GeV in the left panel, while these samples are numerous in the right board. The primary reason for these distinctions is that the electron $g - 2$ anomaly prefers the involved particles, such as the winolike and higgsinolike electroweakinos and $\tilde{e}_L$, to be lighter than the muon $g - 2$ anomaly.

TABLE IV. The numbers of the blue and green samples in Fig. 1, classified by the DM annihilation mechanisms.

	Numbers of the blue samples		Numbers of the green samples	
Annihilation mechanism	Left panel	Right panel	Left panel	Right panel
All	19178	19562	8736	1398
Bino-Wino coannihilation	16415	15506	8627	1327
Bino-Slepton coannihilation	1514	2531	109	71
Z-funnel	691	993	0	0
h-funnel	558	532	0	0

It is remarkable that the bound of $|m_{\tilde{\chi}_1^0}| \gtrsim 275$ GeV, set by the LHC search for SUSY, in the left panel of Fig. 1 is significantly higher than that of $|m_{\tilde{\chi}_1^0}| \gtrsim 224$ GeV in the right board. This conclusion seems unreasonable since the LHC restrictions are tighter for the right panel (see the following discussions). The reason is that we studied the restrictions by simulating the signals of the samples acquired in the scan. So these lower bounds depend on the obtained parameter points or, more basically, their posterior distribution. Given that the points are relatively sparsely distributed in the low $|m_{\tilde{\chi}_1^0}|$ region from 100 GeV to 250 GeV in the left panel, compared with the corresponding area in the right panel, the studied situations are too limited to obtain an accurate bound on $|m_{\tilde{\chi}_1^0}|$. To testify to this speculation, we took the prior of M_1 in Table I to be log distributed and repeated the study of Ref. [159]. We accumulated lots of samples in the low $|m_{\tilde{\chi}_1^0}|$ region and obtained a bound of $|m_{\tilde{\chi}_1^0}| \gtrsim 220$ GeV by concrete MC simulations. This bound came from the experimental analyses in Fig. 16 of Ref. [165], which concluded no LHC restrictions on winos in the $\tilde{B} - \tilde{W}$ co-annihilation case if $m_{\tilde{\chi}_1^0} \gtrsim 220$ GeV. It is a physical bound, independent of the posterior distributions. We add that the lower bound of $|m_{\tilde{\chi}_1^0}|$ yielded in this study is very close to this experimental limit.

(ii) The LHC restrictions on the SUSY explanation. In Table IV, we listed the numbers of the samples plotted in Fig. 1. We classified them by the DM annihilation mechanisms and whether they passed the LHC restrictions. These numbers are approximately proportional to the posterior probabilities of the corresponding samples, and they reflect the LHC's capability to exclude the SUSY parameter points. They indicate that the impacts of the LHC restrictions were more important for this work than for that in Ref. [159]. This conclusion arises from two physical reasons. One is that the electron $g - 2$ anomaly prefers lighter electroweakinos than the muon $g - 2$ anomaly. The other is due to the additional presence of light electron-type sleptons, which

are copiously produced at the LHC and thus enhance the SUSY signals.

We emphasize that the origin of the shared features has been studied in Ref. [159]. By contrast, the differences induced by the addition of the electron anomaly into the likelihood function were not noticed in the literature. Revealing their underlying reasons is the focus of this study.

C. Impacts of the LZ limits on the $\mathbb{Z}_3$-NMSSM

In the last section, we used the XENON-1T results to set upper limits on the SI and SD cross sections of the DM-nucleon scattering [194,195]. These restrictions, however, have been significantly improved by the recent LZ experiment [163]. Given this advancement, we refined the samples in the right panel of Fig. 1 with the LZ restrictions. After projecting the surviving parameter points onto various planes of SUSY parameters and comparing the resulting figures with their initial ones, we acquired the impacts of the LZ experiment on the $\mathbb{Z}_3$-NMSSM. Specifically, we found that most of the similarities in Sec. III B were retained except for the following three remarkable changes:

(i) Given the measured DM density, the LZ experiment alone required $\mu \gtrsim 380$ GeV for $|m_{\tilde{\chi}_1^0}| \simeq 100$ GeV. This lower bound rose as $|m_{\tilde{\chi}_1^0}|$ increased, improving the corresponding XENON-1T restrictions by more than 50 GeV. This feature was shown in Fig. 2. Its primary reason was that an enhanced μ could reduce the $\tilde{\chi}_1^0 \tilde{\chi}_1^0 Z$ and $\tilde{\chi}_1^0 \tilde{\chi}_1^0 h$ coupling strengthes and thus suppress the SI and SD scattering cross sections [234].

(ii) As Fig. 2 of this work indicated, the LZ experiment made the Z-mediated resonant annihilation less preferred. The reason was that with the decrease of the $\tilde{\chi}_1^0 \tilde{\chi}_1^0 Z$ coupling strength, $2|m_{\tilde{\chi}_1^0}|$ should be closer to m_Z to obtain the measured density. This situation required the fine-tuning quantity defined in Eq. (19) of Ref. [191] to be larger than 150. It usually led to the neglect of the resonant annihilation scenario in any less elaborated scan. This conclusion also applied to the h-mediated resonant annihilation. We add that this point was discussed by the Bayesian statistics in footnote 6 of Ref. [161].

One may rephrase this phenomenon as follows: since the relic density and the DM-nucleon scattering
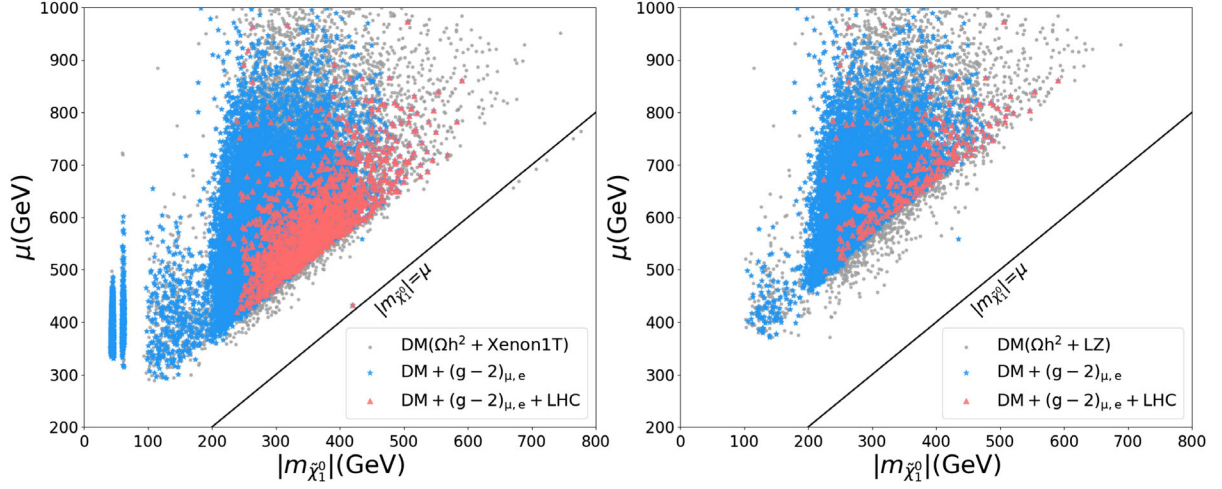
FIG. 2. Left panel: Same as the right panel of Fig. 1, except that the samples are projected onto the $|m_{\tilde{\chi}_1^0}| - \mu$ plane. Right panel: Same as the left panel of this figure, except that all the parameter points further satisfy the LZ restrictions.

cross-sections are highly correlated in the Z- and h-funnel regions, great fine tunings of pertinent SUSY parameters are needed to acquire the measured density and satisfy the restrictions of the DM direct detection experiments simultaneously. This problem becomes more and more severe as the sensitivities of the direct detection experiments are improved.

(iii) Since the LZ and LHC restrictions were sensitive to different SUSY parameters, they complemented each other in probing the parameter space of the $\mathbb{Z}_3$-NMSSM. It was particularly so if one intended to explain the leptonic $g - 2$ anomalies at the 2σ level, because μ was correlated with the other parameters by the anomalies, and any enhancement of μ in a massive higgsino scenario would make winos and $\tilde{\ell}_L$ lighter to keep a_ℓ^{SUSY} unchanged. This situation usually tightens the LHC restrictions.

In Table V, we listed the numbers of the parameter points in the right panel of Fig. 2. Comparing them with the corresponding ones in the left panel of that figure, presented in Table IV, one could readily conclude that, on the premise of explaining the leptonic anomalies at the 2σ level, the LZ experiment significantly promoted the LHC experiments to limit the parameter space of the $\mathbb{Z}_3$-NMSSM.

We point out that these conclusions can also be acquired from an independent scan similar to that in Sec. III B but using the LZ experiment to limit the samples. These two research methods are equivalent because all the considered samples satisfy the LZ restrictions and are derived from the same likelihood function presented in Sec. III A.

Next, we focus on the sparticle mass spectra preferred by the leptonic anomalies, which were plotted in Fig. 3. Through comparing the normalized mass distributions before and after including the LHC restrictions (corresponding to the left and right sides of the violin diagram for each particle in Fig. 3), we conclude that the LHC restrictions affect little the shape of $m_{\tilde{\chi}_5^0}$ and $m_{\tilde{\mu}_R}$ distributions, but prefer more massive $\tilde{\chi}_1^0$, $\tilde{\chi}_2^0$, $\tilde{\chi}_3^0$, $\tilde{\chi}_1^\pm$, $\tilde{\chi}_2^\pm$, $\tilde{e}_L$, $\tilde{e}_R$, and $\tilde{\mu}_L$. The favored mass ranges for the latter set of particles are $600~\mathrm{GeV} \gtrsim m_{\tilde{\chi}_1^0} \gtrsim 224~\mathrm{GeV}$, $m_{\tilde{\chi}_2^0}, m_{\tilde{\chi}_1^\pm} \gtrsim 240~\mathrm{GeV}$, $m_{\tilde{\chi}_3^0} \gtrsim 510~\mathrm{GeV}$, $m_{\tilde{\chi}_4^0}, m_{\tilde{\chi}_2^\pm} \gtrsim 520~\mathrm{GeV}$, $m_{\tilde{\mu}_2} \gtrsim 250~\mathrm{GeV}$, $m_{\tilde{e}_L} \gtrsim 240~\mathrm{GeV}$, $m_{\tilde{e}_R} \gtrsim 230~\mathrm{GeV}$, $m_{\tilde{\mu}_L} \gtrsim 250~\mathrm{GeV}$, and $m_{\tilde{\mu}_R} \gtrsim 230~\mathrm{GeV}$, where the upper bound comes from the requirement to explain the leptonic $g - 2$ anomalies [156]. We verified that $\tilde{\chi}_2^0$ and $\tilde{\chi}_1^\pm$ were wino-dominated when lighter than 500 GeV, and $\tilde{\chi}_5^0$ was always singlino-dominated. We emphasize that these ranges should be regarded as rough estimates rather than accurate

TABLE V. The numbers of the blue and green samples in the right panel of Fig. 2, classified by the DM annihilation mechanisms. This table reflects the LHC's capability to exclude the SUSY parameter points that survive the LZ restrictions.

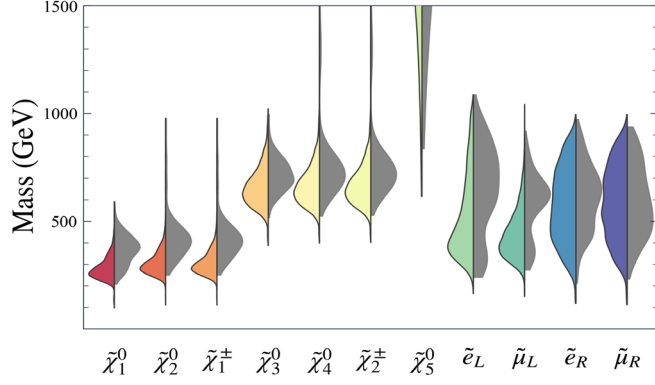| Annihilation mechanisms	Numbers of the blue samples	Numbers of the green samples
All	9180	277
Bino-Wino coannihilation	8372	245
Bino-Sleptons coannihilation	808	32
Z-funnel	0	0
h-funnel	0	0

FIG. 3. Split violin plots with their shapes showing the mass distributions of the particles beyond the SM. This figure is plotted by counting the number of the samples yielded by the scan of this work with the LZ restrictions implemented. The left colorful side and the right gray side of each violin are based on 9188 and 277 samples, respectively. They are marked by the blue triangle and green star in the right panel of Fig. 2. The widths of both sides are fixed so that their ratio does not represent the relative sample number.

bounds since the studied samples need more, given the broad parameter space of the $\mathbb{Z}_3$-NMSSM.

Finally, we have two comments on the acquired results:

(i) Throughout this study, we did not consider the theoretical uncertainties incurred by the simulations and the experimental (systematic and statistical) uncertainties. These effects could relax the LHC restrictions. However, given the advent of the high-luminosity LHC, much tighter restrictions on the $\mathbb{Z}_3$-NMSSM are expected to be available soon.

(ii) In some high-energy SUSY-breaking theories, $\tilde{\tau}$ may be the next-to-lightest supersymmetric particle. In this case, the signatures of the electroweakinos will

significantly differ from those of this study. As a result, the LHC restrictions and, subsequently, the explanation of the anomalies may exhibit new features (see, e.g., the discussion in [123]). We will discuss such a possibility in the future.

D. Predictions of a_e^{SUSY} in the $\mathbb{Z}_3$-NMSSM

To learn the typical size of a_e^{SUSY} in the $\mathbb{Z}_3$-NMSSM, we projected the parameter points yielded by the scan of this work onto the a_μ^{SUSY}—a_e^{SUSY} plane. The results were shown in Fig. 4, where the samples in the left panel coincided with the XENON-1T results, while those in the right board further satisfied the LZ restrictions. This figure revealed the following features:

(i) The formula $a_e^{\text{SUSY}}/m_e^2 \simeq a_\mu^{\text{SUSY}}/m_\mu^2$ correlated a_e^{SUSY} and a_μ^{SUSY} in most cases. The primary reason was that the two quantities depended similarly on the parameters M_1, M_2, and μ, and meanwhile, the electron-type and muon-type sleptons were comparable in mass. Consequently, a_e^{SUSY} was typically around 5×10^{-14} when $a_\mu^{\text{SUSY}} \simeq 2.5 \times 10^{-9}$. In addition, we found the violations of this correlation in rare cases such as $m_{\tilde{\mu}_L} \gg M_2, \mu, m_{\tilde{e}_L}$, where a_e^{SUSY}/m_e^2 could be much larger than $a_\mu^{\text{SUSY}}/m_\mu^2$.

(ii) The DM direct detection experiments and the LHC experiments were tight in restricting the case of $a_e^{\text{SUSY}} \gtrsim 1.0 \times 10^{-13}$ or $a_\mu^{\text{SUSY}} \gtrsim 3.0 \times 10^{-9}$, where some sparticles involved in the leptonic anomalies should be relatively light, as revealed by the discussions of this study. This fact implied that a_e^{SUSY} and a_μ^{SUSY} could not be huge. Specifically, a_e^{SUSY} and a_μ^{SUSY} might reach 3×10^{-13} and 5×10^{-9}, respectively, in the optimum cases if one used the
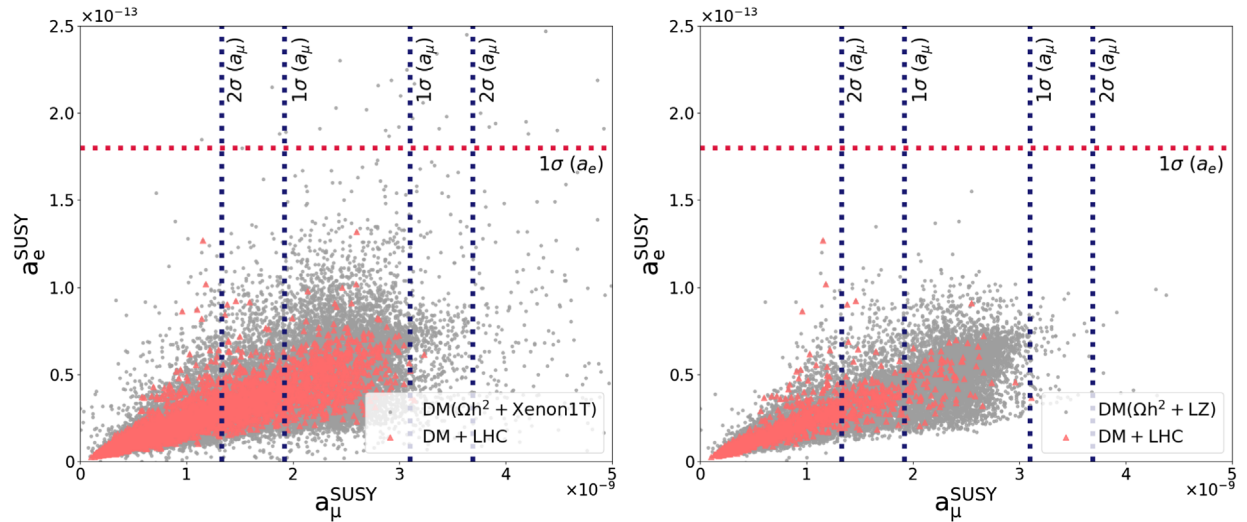

FIG. 4. Similar to Fig. 2, except that the samples are projected onto the a_μ^{SUSY}—a_e^{SUSY} planes. The red dashed line corresponds to the 1σ lower bound of a_e^{SUSY}, and the black dashed lines are the 1σ and 2σ bounds of a_μ^{SUSY}. To acquire this figure, we especially included the samples predicting $a_e^{\text{SUSY}} > 0$ and $0 < a_\mu^{\text{SUSY}} \leq 13.3 \times 10^{-10}$ and simulated their signals at the LHC.

TABLE VI.   Details of two benchmark points, P1 and P2. Both points predict $a_\mu^{\mathrm{SUSY}} \simeq 2.5 \times 10^{-9}$, but they correspond to significantly different a_e^{SUSY}.

Benchmark Point P1				Benchmark Point P2			
λ	0.151	m_{h_s}	961.7 GeV	λ	0.23	m_{h_s}	2450.5 GeV
κ	0.218	m_{A_s}	1166.4 GeV	κ	0.53	m_{A_s}	914.3 GeV
$\tan\beta$	38.7	m_h	124.7 GeV	$\tan\beta$	28.9	m_h	124.7 GeV
μ	407.7 GeV	m_{A_H}	6258.3 GeV	μ	541.4 GeV	m_{A_H}	7047.0 GeV
A_t	-3045.8 GeV	$m_{\tilde\chi_1^0}$	60.3 GeV	A_t	-2957.5 GeV	$m_{\tilde\chi_1^0}$	-254.8 GeV
A_κ	-776.7 GeV	$m_{\tilde\chi_2^0}$	175.5 GeV	A_κ	-231.0 GeV	$m_{\tilde\chi_2^0}$	277.4 GeV
M_1	61.3 GeV	$m_{\tilde\chi_3^0}$	-425.7 GeV	M_1	-256.3 GeV	$m_{\tilde\chi_3^0}$	-561.1 GeV
M_2	171.9 GeV	$m_{\tilde\chi_4^0}$	434.0 GeV	M_2	270.0 GeV	$m_{\tilde\chi_4^0}$	566.9 GeV
$M_{\tilde e_L}$	127.1 GeV	$m_{\tilde\chi_5^0}$	1176.5 GeV	$M_{\tilde e_L}$	124.8 GeV	$m_{\tilde\chi_5^0}$	2521.3 GeV
$M_{\tilde e_R}$	573.0 GeV	$m_{\tilde\chi_1^\pm}$	175.7 GeV	$M_{\tilde e_R}$	805.4 GeV	$m_{\tilde\chi_1^\pm}$	277.6 GeV
$M_{\tilde\mu_L}$	663.2 GeV	$m_{\tilde\chi_2^\pm}$	437.2 GeV	$M_{\tilde\mu_L}$	278.5 GeV	$m_{\tilde\chi_2^\pm}$	570.0 GeV
$M_{\tilde\mu_R}$	707.6 GeV	$m_{\tilde e_L}$	256.0 GeV	$M_{\tilde\mu_R}$	767.0 GeV	$m_{\tilde e_L}$	287.3 GeV
a_e^{SUSY}	2.66×10^{-13}	$m_{\tilde e_R}$	487.7 GeV	a_e^{SUSY}	6.8×10^{-14}	$m_{\tilde e_R}$	725.4 GeV
a_μ^{SUSY}	2.44×10^{-9}	$m_{\tilde\mu_L}$	700.6 GeV	a_μ^{SUSY}	2.51×10^{-9}	$m_{\tilde\mu_L}$	381.2 GeV
Ωh^2	0.14	$m_{\tilde\mu_R}$	641.1 GeV	Ωh^2	0.10	$m_{\tilde\mu_R}$	683.0 GeV
σ_p^{SI}	3.40×10^{-47} cm^2	$m_{\tilde\nu_e}$	243.9 GeV	σ_p^{SI}	5.98×10^{-47} cm^2	$m_{\tilde\nu_e}$	276.7 GeV
σ_n^{SD}	3.95×10^{-42} cm^2	$m_{\tilde\nu_\mu}$	695.8 GeV	σ_n^{SD}	1.74×10^{-42} cm^2	$m_{\tilde\nu_\mu}$	373.3 GeV

$N_{11}, N_{12}, N_{13}, N_{14}, N_{15}$	$-0.994, 0.014, -0.109, 0.019, -0.003$	$N_{11}, N_{12}, N_{13}, N_{14}, N_{15}$	$-0.994, -0.006, -0.097, -0.042, -0.002$
$N_{21}, N_{22}, N_{23}, N_{24}, N_{25}$	$-0.039, -0.970, 0.219, -0.096, 0.006$	$N_{21}, N_{22}, N_{23}, N_{24}, N_{25}$	$0.009, 0.978, -0.187, 0.098, -0.003$
$N_{31}, N_{32}, N_{33}, N_{34}, N_{35}$	$-0.062, 0.090, 0.697, 0.709, 0.011$	$N_{31}, N_{32}, N_{33}, N_{34}, N_{35}$	$0.098, -0.064, -0.698, -0.706, -0.009$
$N_{41}, N_{42}, N_{43}, N_{44}, N_{45}$	$0.084, -0.225, -0.674, 0.699, -0.023$	$N_{41}, N_{42}, N_{43}, N_{44}, N_{45}$	$0.038, -0.201, -0.684, 0.700, -0.013$
$N_{51}, N_{52}, N_{53}, N_{54}, N_{55}$	$-0.001, -0.001, -0.025, 0.008, 0.999$	$N_{51}, N_{52}, N_{53}, N_{54}, N_{55}$	$-0.001, -0.000, -0.016, 0.003, 1.000$

Annihilations	Fractions[%]	Annihilations	Fractions[%]
$\tilde\chi_1^0 \tilde\chi_1^0 \to f\bar f/gg$	82.8/17.2	$\tilde B - \tilde W$ Co-annihilation	100

Decays	Branching ratios[%]	Decays	Branching ratios[%]
$\tilde\chi_2^0 \to \tilde\chi_1^0 Z$	98.1	$\tilde\chi_2^0 \to \tilde\nu_e \nu_e$	99.5
$\tilde\chi_3^0 \to \tilde\chi_1^\pm W^\mp/\tilde\chi_2^0 Z/\tilde\chi_1^0 Z/\tilde\chi_1^0 h/\tilde\chi_2^0 h$	62.1/23.8/7.4/3.3/2.9	$\tilde\chi_3^0 \to \tilde\chi_1^\pm W^\mp/\tilde\chi_2^0 Z/\tilde\chi_1^0 h/\tilde\chi_2^0 h/\tilde\chi_1^0 Z$	61.6/26.4/7.4/2.2/1.4
$\tilde\chi_4^0 \to \tilde\chi_1^\pm W^\mp/\tilde\chi_2^0 h/\tilde\chi_1^0 h/\tilde\chi_2^0 Z$ $/\tilde\chi_1^0 Z/\tilde\nu_e \nu_e/\tilde e_L^\pm e^\mp$	62.6/19.9/6.2/4.4/3.6/2.4/1.0	$\tilde\chi_4^0 \to \tilde\chi_1^\pm W^\mp/\tilde\chi_2^0 h/\tilde\chi_1^0 Z/\tilde\chi_2^0 Z/\tilde\nu_e \nu_e$ $/\tilde e_L^\pm e^\mp/\tilde\nu_\mu \nu_\mu/\tilde\chi_1^0 h$	60.6/23.3/7.1/3.0/1.9/1.2/1.1/1.1
$\tilde\chi_5^0 \to \tilde\chi_2^\pm W^\mp/\tilde\chi_4^0 h/\tilde\chi_3^0 Z/\tilde\chi_3^0 h$ $/\tilde\chi_1^\pm W^\mp//\tilde\chi_4^0 Z/\tilde\chi_2 h/\tilde\chi_2 Z$	44.3/19.2/18.8/4.8/4.6/4.2/1.3/1.1	$\tilde\chi_5^0 \to \tilde\chi_2^\pm W^\mp/\tilde\chi_4^0 h/\tilde\chi_3^0 Z/\tilde\chi_3^0 h/\tilde\chi_4^0 Z$ $/\tilde\chi_1^\pm W^\mp/\tilde\chi_2^0 h$	44.7/16.1/15.9/7.8/7.0/3.3/1.0
$\tilde\chi_1^\pm \to \tilde\chi_1^0 W^\pm$	99.4	$\tilde\chi_1^\pm \to \tilde\nu_e e^\mp$	99.8
$\tilde\chi_2^\pm \to \tilde\chi_2^0 W^\pm/\tilde\chi_1^\pm Z/\tilde\chi_1^\pm h$ $/\tilde\chi_1^0 W^\pm/\tilde e_L \nu_e$	32.7/29.7/24.1/9.9/3.0	$\tilde\chi_2^\pm \to \tilde\chi_2^0 W^\pm/\tilde\chi_1^\pm Z/\tilde\chi_1^\pm h/\tilde\chi_1^0 W^\pm$ $/\tilde e_L^\pm \nu_e/\tilde\mu_L^\pm \nu_\mu$	30.6/29.2/25.6/9.3/2.6/1.5
$\tilde e_L^\pm \to \tilde\chi_1^0 \nu_e/\tilde\chi_2^0 e^\pm/\tilde\chi_1^0 e^\pm$	48.2/25.4/26.4	$\tilde e_L^\pm \to \tilde\chi_1^0 e^\pm/\tilde\chi_1^\pm \nu_e/\tilde\chi_2^0 e^\pm$	53.7/29.9/16.4
$\tilde e_R^\pm \to \tilde\chi_1^0 e^\pm$	99.8	$\tilde e_R^\pm \to \tilde\chi_1^0 e^\pm$	99.7
$\tilde\mu_L^\pm \to \tilde\chi_1^\pm \nu_\mu/\tilde\chi_2^0 \mu^\pm/\tilde\chi_1^0 \mu^\pm/\tilde\chi_2^\pm \nu_\mu$	56.0/30.5/10.4/2.5	$\tilde\mu_L^\pm \to \tilde\chi_1^\pm \nu_\mu/\tilde\chi_2^0 \mu^\pm/\tilde\chi_1^0 \mu^\pm$	56.8/29.6/13.6
$\tilde\mu_R^\pm \to \tilde\chi_1^0 \mu^\pm$	99.2	$\tilde\mu_R^\pm \to \tilde\chi_1^0 \mu^\pm$	99.6
$\tilde\nu_e \to \tilde\chi_1^\pm e^\mp/\tilde\chi_1^0 \nu_e/\tilde\chi_2^0 \nu_e$	47.6/30.5/21.9	$\tilde\nu_e \to \tilde\chi_1^\pm e^\mp$	100
$\tilde\nu_\mu \to \tilde\chi_1^\pm \mu^\mp/\tilde\chi_2^0 \nu_\mu/\tilde\chi_1^0 \nu_\mu/\tilde\chi_4^0 \nu_\mu$	59.7/27.3/11.3/1.0	$\tilde\nu_\mu \to \tilde\chi_1^\pm \mu^\mp/\tilde\chi_2^0 \nu_\mu/\tilde\chi_1^0 \nu_\mu$	58.5/28.3/13.2
R value	4.83, ATLAS-SUSY-2018-06	R value	0.75, CMS-SUS-20-001

XENON-1T experiment to limit the SUSY parameter space. The predictions, however, reduced to 1.5×10^{-13} and 4×10^{-9} correspondingly after implementing the LZ restrictions and 1.0×10^{-13} and 3×10^{-9} when further considering the LHC restrictions.

In Table VI, we provided the details of two benchmark points, P1 and P2, both predicting $a_\mu^{\mathrm{SUSY}} \simeq 2.5 \times 10^{-9}$. Point P1 corresponded to a relatively large a_e^{SUSY}, i.e., $a_e^{\mathrm{SUSY}} \simeq 2.7 \times 10^{-13}$. It satisfied the XENON-1T restrictions but was excluded by

the LZ and LHC experiments. By contrast, a_e^{SUSY} of point P2 was moderate, namely $a_e^{\text{SUSY}} = 6.8 \times 10^{-14}$, and this point coincided with all the experimental results.

IV. SUMMARY

In recent years we have witnessed the rapid progress of particle physics experiments. In particular, the discrepancy between a_μ^{Exp} and a_μ^{SM} was corroborated by the E989 experiment at FNAL, and the significant departures of a_e^{Exp} from a_e^{SM} were also observed in the measurements of the fine structure constant at LKB and LBNL. These anomalies hinted at the existence of new physics, and SUSY as the most compelling new physics candidate has attracted a lot of attention.

So far, most of the studies on the leptonic anomalies concentrated on the MSSM, which, however, suffered increasing fine-tuning problems as the smooth ongoing of the LHC experiments. This situation motivated us to explore this subject in another economic and self-contained low-energy realization of SUSY, namely the $\mathbb{Z}_3$-NMSSM. Specifically, we investigated how large a_e^{SUSY} could reach in the $\mathbb{Z}_3$-NMSSM after considering various experimental restrictions, given that this quantity was scarcely studied in SUSY. For this purpose, we utilized the MultiNest algorithm to scan the theory's parameter space comprehensively. We adopted the leptonic anomalies to guide the scans and included the restrictions from the LHC Higgs data, the DM relic density, the DM direct detection by the XENON-1T experiments, the B-physics measurements, and the vacuum stability. We also scrutinized the samples acquired in the scans with the restrictions from the LHC search for SUSY and the latest LZ experiment. We obtained the conclusions mainly concerning the DM annihilation mechanisms to achieve the measured DM density and the substantial restrictions of the LHC search for SUSY and the DM direct detections on the parameter space. Most of these conclusions are the same as those in Ref. [159], which similarly studied the muon $g - 2$ anomaly in the $\mathbb{Z}_3$-NMSSM. However, we still had new observations, summarized as follows:

(i) a_e^{SUSY} was mainly correlated with a_μ^{SUSY} by the formula $a_e^{\text{SUSY}}/m_e^2 \simeq a_\mu^{\text{SUSY}}/m_\mu^2$ because the two quantities depended similarly on the parameters M_1, M_2, and μ, and meanwhile, the electron-type and muon-type sleptons were comparable in mass. As a result, a_e^{SUSY} was typically around 5×10^{-14} when $a_\mu^{\text{SUSY}} \simeq 2.5 \times 10^{-9}$. In addition, significant violations of this correlation might occur only in rare cases such as $m_{\tilde{\mu}_L} \gg M_2, \mu, m_{\tilde{e}_L}$, where a_e^{SUSY}/m_e^2 could be much larger than $a_\mu^{\text{SUSY}}/m_\mu^2$.

(ii) The DM direct detection and LHC experiments were more crucial in determining the results of this work than those in Ref. [159]. This conclusion was reflected not only by the percentages of the samples excluded by the restrictions, which were presented in Tables IV and V, but also by the maximum reach of a_e^{SUSY}. Concretely, a_e^{SUSY} might be around 3×10^{-13} in the optimum cases if one used the XENON-1T experiment to limit the SUSY parameter space. This prediction, however, was reduced to 1.5×10^{-13} after implementing the LZ restrictions and 1.0×10^{-13} when further considering the LHC restrictions. The underlying reason for this phenomenon is that the electron $g - 2$ anomaly prefers lighter electroweakinos than the muon $g - 2$ anomaly. It also requires the presence of light electron-type sleptons. The experiments have tightly limited these situations.

(iii) On the premise of predicting $a_e^{\text{SUSY}} > 0$ and explaining the muon $g - 2$ anomaly at the 2σ level, the LHC restrictions have set lower bounds on the sparticle mass spectra, e.g., $m_{\tilde{\chi}_1^0} \gtrsim 220$ GeV and $m_{\tilde{\chi}_2^0}, m_{\tilde{\chi}_1^\pm} \gtrsim 240$ GeV, where $\tilde{\chi}_2^0$ and $\tilde{\chi}_1^\pm$ are wino-dominated. Remarkably, although these lower bounds depended on the obtained parameter points or, more basically, their posterior distribution, our results coincided with those from the experimental analyses in Fig. 16 of Ref. [165], which concluded no LHC restrictions on winos in the $\tilde{B} - \tilde{W}$ co-annihilation case if $m_{\tilde{\chi}_1^0} \gtrsim 220$ GeV. The reason was that we accumulated lots of samples in the low $|m_{\tilde{\chi}_1^0}|$ region in the right panel of Fig. 1 and thus explored numerous situations of SUSY.

These bounds can be understood intuitively as follows: if $\tilde{\chi}_1^0$ is lighter, more missing transverse energy will be emitted in the sparticle production processes at the LHC, which can improve the sensitivities of the experimental analyses; while if the sparticles other than $\tilde{\chi}_1^0$ are lighter, they will be more copiously produced at the LHC to increase the events containing multiple leptons.

(iv) Since the relic density was highly correlated with the DM-nucleon scattering cross-sections in the Z- and h-funnel regions, one needed great fine tunings of relevant SUSY parameters to yield the measured density without conflicting with the restrictions of the DM direct detection experiments. This problem became more and more severe with the improvement of the sensitivities of the direct detection experiments. As a result, these annihilation scenarios were usually neglected if not focused on in a parameter scan utilizing the MultiNest algorithm and considering the LZ restrictions.

ACKNOWLEDGMENTS

[1] B. Abi *et al.* (Muon $g - 2$ Collaboration), Measurement of the Positive Muon Anomalous Magnetic Moment to 0.46 ppm, Phys. Rev. Lett. **126,** 141801 (2021).

[2] G. W. Bennett *et al.* (Muon $g - 2$ Collaboration), Final report of the muon E821 anomalous magnetic moment measurement at BNL, Phys. Rev. D **73,** 072003 (2006).

[3] T. Aoyama *et al.*, The anomalous magnetic moment of the muon in the standard model, Phys. Rep. **887,** 1 (2020).

[4] T. Aoyama, M. Hayakawa, T. Kinoshita, and M. Nio, Complete Tenth-Order QED Contribution to the Muon $g - 2$, Phys. Rev. Lett. **109,** 111808 (2012).

[5] T. Aoyama, T. Kinoshita, and M. Nio, Theory of the anomalous magnetic moment of the electron, Atoms **7,** 28 (2019).

[6] A. Czarnecki, W. J. Marciano, and A. Vainshtein, Refinements in electroweak contributions to the muon anomalous magnetic moment, Phys. Rev. D **67,** 073006 (2003).

[7] C. Gnendiger, D. Stöckinger, and H. Stöckinger-Kim, The electroweak contributions to $(g - 2)_\mu$ after the Higgs boson mass measurement, Phys. Rev. D **88,** 053005 (2013).

[8] M. Davier, A. Hoecker, B. Malaescu, and Z. Zhang, Reevaluation of the hadronic vacuum polarisation contributions to the standard model predictions of the muon $g - 2$ and $\alpha(m_Z^2)$ using newest hadronic cross-section data, Eur. Phys. J. C **77,** 827 (2017).

[9] A. Keshavarzi, D. Nomura, and T. Teubner, Muon $g - 2$ and $\alpha(M_Z^2)$: A new data-based analysis, Phys. Rev. D **97,** 114025 (2018).

[10] G. Colangelo, M. Hoferichter, and P. Stoffer, Two-pion contribution to hadronic vacuum polarization, J. High Energy Phys. 02 (2019) 006.

[11] M. Hoferichter, B.-L. Hoid, and B. Kubis, Three-pion contribution to hadronic vacuum polarization, J. High Energy Phys. 08 (2019) 137.

[12] M. Davier, A. Hoecker, B. Malaescu, and Z. Zhang, A new evaluation of the hadronic vacuum polarisation contributions to the muon anomalous magnetic moment and to $\boldsymbol{\alpha(m_Z^2)}$, Eur. Phys. J. C **80,** 241 (2020).

[13] A. Keshavarzi, D. Nomura, and T. Teubner, The $g - 2$ of charged leptons, $\alpha(M_Z^2)$ and the hyperfine splitting of muonium, Phys. Rev. D **101,** 014029 (2020).

[14] A. Kurz, T. Liu, P. Marquard, and M. Steinhauser, Hadronic contribution to the muon anomalous magnetic moment to next-to-next-to-leading order, Phys. Lett. B **734,** 144 (2014).

[15] K. Melnikov and A. Vainshtein, Hadronic light-by-light scattering contribution to the muon anomalous magnetic moment revisited, Phys. Rev. D **70,** 113006 (2004).

[16] P. Masjuan and P. Sánchez-Puertas, Pseudoscalar-pole contribution to the $(g_\mu - 2)$: A rational approach, Phys. Rev. D **95,** 054026 (2017).

[17] G. Colangelo, M. Hoferichter, M. Procura, and P. Stoffer, Dispersion relation for hadronic light-by-light scattering: Two-pion contributions, J. High Energy Phys. 04 (2017) 161.

[18] M. Hoferichter, B.-L. Hoid, B. Kubis, S. Leupold, and S. P. Schneider, Dispersion relation for hadronic light-by-light scattering: Pion pole, J. High Energy Phys. 10 (2018) 141.

[19] A. Gérardin, H. B. Meyer, and A. Nyffeler, Lattice calculation of the pion transition form factor with $N_f = 2 + 1$ Wilson quarks, Phys. Rev. D **100,** 034520 (2019).

[20] J. Bijnens, N. Hermansson-Truedsson, and A. Rodríguez-Sánchez, Short-distance constraints for the HLbL contribution to the muon anomalous magnetic moment, Phys. Lett. B **798,** 134994 (2019).

[21] G. Colangelo, F. Hagelstein, M. Hoferichter, L. Laub, and P. Stoffer, Longitudinal short-distance constraints for the hadronic light-by-light contribution to $(g - 2)_\mu$ with large-N_c Regge models, J. High Energy Phys. 03 (2020) 101.

[22] T. Blum, N. Christ, M. Hayakawa, T. Izubuchi, L. Jin, C. Jung, and C. Lehner, The Hadronic Light-by-Light Scattering Contribution to the Muon Anomalous Magnetic Moment from Lattice QCD, Phys. Rev. Lett. **124,** 132002 (2020).

[23] G. Colangelo, M. Hoferichter, A. Nyffeler, M. Passera, and P. Stoffer, Remarks on higher-order hadronic corrections to the muon $g - 2$, Phys. Lett. B **735,** 90 (2014).

[24] S. Borsanyi *et al.*, Leading hadronic contribution to the muon magnetic moment from lattice QCD, Nature (London) **593,** 51 (2021).

[25] C. Alexandrou *et al.*, Lattice calculation of the short and intermediate time-distance hadronic vacuum polarization contributions to the muon magnetic moment using twisted-mass fermions, Phys. Rev. D **107,** 074506 (2023).

[26] M. Cè *et al.*, Window observable for the hadronic vacuum polarization contribution to the muon $g - 2$ from lattice QCD, Phys. Rev. D **106,** 114502 (2022).

[27] A. Crivellin, M. Hoferichter, C. A. Manzari, and M. Montull, Hadronic Vacuum Polarization: $(g - 2)_\mu$ versus Global Electroweak Fits, Phys. Rev. Lett. **125,** 091801 (2020).

[28] G. Colangelo, A. X. El-Khadra, M. Hoferichter, A. Keshavarzi, C. Lehner, P. Stoffer, and T. Teubner, Data-driven evaluations of Euclidean windows to scrutinize hadronic vacuum polarization, Phys. Lett. B **833,** 137313 (2022).

[29] E. de Rafael, Constraints between $\Delta\alpha_{\text{had}}(M_Z^2)$ and $(g_\mu - 2)_{\text{HVP}}$, Phys. Rev. D **102,** 056025 (2020).

[30] A. Keshavarzi, W. J. Marciano, M. Passera, and A. Sirlin, Muon $g - 2$ and $\Delta\alpha$ connection, Phys. Rev. D **102,** 033002 (2020).

[31] T. Albahri *et al.* (Muon $g - 2$ Collaboration), Measurement of the anomalous precession frequency of the muon in the Fermilab Muon $g - 2$ Experiment, Phys. Rev. D **103,** 072002 (2021).

[32] M. Abe *et al.*, A new approach for measuring the muon anomalous magnetic moment and electric dipole moment, Prog. Theor. Exp. Phys. **2019,** 053C02 (2019).

[33] L. Morel, Z. Yao, P. Cladé, and S. Guellati-Khélifa, Determination of the fine-structure constant with an accuracy of 81 parts per trillion, Nature (London) **588,** 61 (2020).

[34] D. Hanneke, S. Fogwell, and G. Gabrielse, New Measurement of the Electron Magnetic Moment and the Fine Structure Constant, Phys. Rev. Lett. **100,** 120801 (2008).

[35] R. H. Parker, C. Yu, W. Zhong, B. Estey, and H. Müller, Measurement of the fine-structure constant as a test of the standard model, Science **360,** 191 (2018).

[36] P. Athron, C. Balázs, D. H. Jacob, W. Kotlarski, D. Stöckinger, and H. Stöckinger-Kim, New physics explanations of a_μ in light of the FNAL muon $g-2$ measurement, J. High Energy Phys. 09 (2021) 080.

[37] H. Davoudiasl and W. J. Marciano, Tale of two anomalies, Phys. Rev. D **98,** 075011 (2018).

[38] J. Liu, C. E. M. Wagner, and X.-P. Wang, A light complex scalar for the electron and muon anomalous magnetic moments, J. High Energy Phys. 03 (2019) 008.

[39] M. Bauer, M. Neubert, S. Renner, M. Schnubel, and A. Thamm, Axionlike Particles, Lepton-Flavor Violation, and a New Explanation of a_μ and a_e, Phys. Rev. Lett. **124,** 211803 (2020).

[40] C. Cornella, P. Paradisi, and O. Sumensari, Hunting for ALPs with lepton flavor violation, J. High Energy Phys. 01 (2020) 158.

[41] M. Endo, S. Iguro, and T. Kitahara, Probing $e\mu$ flavor-violating ALP at Belle II, J. High Energy Phys. 06 (2020) 040.

[42] N. Haba, Y. Shimizu, and T. Yamada, Muon and electron $g-2$ and the origin of the fermion mass hierarchy, Prog. Theor. Exp. Phys. **2020,** 093B05 (2020).

[43] R. Adhikari, I. A. Bhat, D. Borah, E. Ma, and D. Nanda, Anomalous magnetic moment and Higgs coupling of the muon in a sequential U(1) gauge model with dark matter, Phys. Rev. D **105,** 035006 (2022).

[44] M. Bauer, M. Neubert, S. Renner, M. Schnubel, and A. Thamm, Flavor probes of axion-like particles, J. High Energy Phys. 09 (2022) 056.

[45] B. De, D. Das, M. Mitra, and N. Sahoo, Magnetic moments of leptons, charged lepton flavor violations and dark matter phenomenology of a minimal radiative Dirac neutrino mass model, J. High Energy Phys. 08 (2022) 202.

[46] C.-K. Chua, Data-driven study of the implications of anomalous magnetic moments and lepton flavor violating processes of e, μ and τ, Phys. Rev. D **102,** 055022 (2020).

[47] S. Gardner and X. Yan, Light scalars with lepton number to solve the $(g-2)_e$ anomaly, Phys. Rev. D **102,** 075016 (2020).

[48] B. Dutta, S. Ghosh, and T. Li, Explaining $(g-2)_{\mu,e}$, the KOTO anomaly and the MiniBooNE excess in an extended Higgs model with sterile neutrinos, Phys. Rev. D **102,** 055017 (2020).

[49] F. J. Botella, F. Cornet-Gomez, and M. Nebot, Electron and muon $g-2$ anomalies in general flavour conserving two Higgs doublets models, Phys. Rev. D **102,** 035023 (2020).

[50] S. Jana, P. K. Vishnu, and S. Saad, Resolving electron and muon $g-2$ within the 2HDM, Phys. Rev. D **101,** 115037 (2020).

[51] X.-F. Han, T. Li, L. Wang, and Y. Zhang, Simple interpretations of lepton anomalies in the lepton-specific inert two-Higgs-doublet model, Phys. Rev. D **99,** 095034 (2019).

[52] A. E. C. Hernández, S. F. King, and H. Lee, Fermion mass hierarchies from vectorlike families with an extended 2HDM and a possible explanation for the electron and muon anomalous magnetic moments, Phys. Rev. D **103,** 115024 (2021).

[53] L. Delle Rose, S. Khalil, and S. Moretti, Explaining electron and muon $g-2$ anomalies in an aligned 2-Higgs

[54] S.-P. Li, X.-Q. Li, Y.-Y. Li, Y.-D. Yang, and X. Zhang, Power-aligned 2HDM: A correlative perspective on $(g-2)_{e,\mu}$, J. High Energy Phys. 01 (2021) 034.

[55] X.-F. Han, T. Li, H.-X. Wang, L. Wang, and Y. Zhang, Lepton-specific inert two-Higgs-doublet model confronted with the new results for muon and electron $g-2$ anomalies and multilepton searches at the LHC, Phys. Rev. D **104,** 115001 (2021).

[56] R. K. Barman, R. Dcruz, and A. Thapa, Neutrino masses and magnetic moments of electron and muon in the Zee model, J. High Energy Phys. 03 (2022) 183.

[57] F. J. Botella, F. Cornet-Gomez, C. Miró, and M. Nebot, Leptonic $g-2$ in 2HDM, in *Proceedings of the 56th Rencontres de Moriond on Electroweak Interactions and Unified Theories* (2022), arXiv:2205.07350.

[58] L. T. Hue, A. E. Cárcamo Hernández, H. N. Long, and T. T. Hong, Heavy singly charged Higgs bosons and inverse seesaw neutrinos as origins of large $(g-2)_{e,\mu}$ in two Higgs doublet models, Nucl. Phys. **B984,** 115962 (2022).

[59] S. Fajfer, J. F. Kamenik, and M. Tammaro, Interplay of new physics effects in $(g-2)_\ell$ and $h \to \ell^+\ell^-$ lessons from SMEFT, J. High Energy Phys. 06 (2021) 099.

[60] A. Crivellin, M. Hoferichter, and P. Schmidt-Wellenburg, Combined explanations of $(g-2)_{\mu,e}$ and implications for a large muon EDM, Phys. Rev. D **98,** 113002 (2018).

[61] E. J. Chun and T. Mondal, Explaining $g-2$ anomalies in two Higgs doublet model with vector-like leptons, J. High Energy Phys. 11 (2020) 077.

[62] K.-F. Chen, C.-W. Chiang, and K. Yagyu, An explanation for the muon and electron $g-2$ anomalies and dark matter, J. High Energy Phys. 09 (2020) 119.

[63] C. Hati, J. Kriewald, J. Orloff, and A. M. Teixeira, Anomalies in ^{8}Be nuclear transitions and $(g-2)_{e,\mu}$: Towards a minimal combined explanation, J. High Energy Phys. 07 (2020) 235.

[64] S. Jana, P. K. Vishnu, W. Rodejohann, and S. Saad, Dark matter assisted lepton anomalous magnetic moments and neutrino masses, Phys. Rev. D **102,** 075003 (2020).

[65] G. Hiller, C. Hormigos-Feliu, D. F. Litim, and T. Steudtner, Anomalous magnetic moments from asymptotic safety, Phys. Rev. D **102,** 071901 (2020).

[66] D. Borah, M. Dutta, S. Mahapatra, and N. Sahu, Lepton anomalous magnetic moment with singlet-doublet fermion dark matter in a scotogenic $U(1)_{L_\mu-L_\tau}$ model, Phys. Rev. D **105,** 015029 (2022).

[67] A. Biswas and S. Khan, $(g-2)_{e,\mu}$ and strongly interacting dark matter with collider implications, J. High Energy Phys. 07 (2022) 037.

[68] F. J. Botella, F. Cornet-Gomez, C. Miró, and M. Nebot, Muon and electron $g-2$ anomalies in a flavor conserving 2HDM with an oblique view on the CDF M_W value, Eur. Phys. J. C **82,** 915 (2022).

[69] H. Bharadwaj, S. Dutta, and A. Goyal, Leptonic g -2 anomaly in an extended Higgs sector with vector-like leptons, J. High Energy Phys. 11 (2021) 056.

[70] A. Crivellin and M. Hoferichter, Combined explanations of $(g-2)_\mu$, $(g-2)_e$ and implications for a large muon EDM, Proc. Sci. ALPS2019 (**2020**) 009.

[71] W.-Y. Keung, D. Marfatia, and P.-Y. Tseng, Axion-like particles, two-Higgs-doublet models, leptoquarks, and the electron and muon $g - 2$, Lett. High Energy Phys. **2021,** 209 (2021).

[72] I. Bigaran and R. R. Volkas, Getting chirality right: Single scalar leptoquark solutions to the $(g - 2)_{e,\mu}$ puzzle, Phys. Rev. D **102,** 075037 (2020).

[73] I. Doršner, S. Fajfer, and S. Saad, $\mu \to e\gamma$ selecting scalar leptoquark solutions for the $(g - 2)_{e,\mu}$ puzzles, Phys. Rev. D **102,** 075007 (2020).

[74] I. Bigaran and R. R. Volkas, Reflecting on chirality: CP-violating extensions of the single scalar-leptoquark solutions for the $(g - 2)_{e,\mu}$ puzzles and their implications for lepton EDMs, Phys. Rev. D **105,** 015002 (2022).

[75] P. Escribano, J. Terol-Calvo, and A. Vicente, $(\boldsymbol{g - 2})_{e,\boldsymbol{\mu}}$ in an extended inverse type-III seesaw model, Phys. Rev. D **103,** 115018 (2021).

[76] T. A. Chowdhury, M. Ehsanuzzaman, and S. Saad, Dark matter and $(g - 2)_{\mu,e}$ in radiative Dirac neutrino mass models, J. Cosmol. Astropart. Phys. 08 (2022) 076.

[77] T. T. Hong, N. H. T. Nha, T. P. Nguyen, L. T. T. Phuong, and L. T. Hue, Decays $h \to eaeb$, $eb \to ea\gamma$, and $(g - 2)_{e,\mu}$ in a 3-3-1 model with inverse seesaw neutrinos, Prog. Theor. Exp. Phys. **2022,** 093B05 (2022).

[78] A. E. C. Hernández, D. T. Huong, and I. Schmidt, Universal inverse seesaw mechanism as a source of the SM fermion mass hierarchy, Eur. Phys. J. C **82,** 63 (2022).

[79] T. Mondal and H. Okada, Inverse seesaw and $(g - 2)$ anomalies in $B - L$ extended two Higgs doublet model, Nucl. Phys. **B976,** 115716 (2022).

[80] C. Arbeláez, R. Cepedello, R. M. Fonseca, and M. Hirsch, $(g - 2)$ anomalies and neutrino mass, Phys. Rev. D **102,** 075005 (2020).

[81] M. Abdullah, B. Dutta, S. Ghosh, and T. Li, $(g - 2)_{\mu,e}$ and the ANITA anomalous events in a three-loop neutrino mass model, Phys. Rev. D **100,** 115006 (2019).

[82] A. E. Cárcamo Hernández, Y. Hidalgo Velásquez, S. Kovalenko, H. N. Long, N. A. Pérez-Julve, and V. V. Vien, Fermion spectrum and $g - 2$ anomalies in a low scale 3-3-1 model, Eur. Phys. J. C **81,** 191 (2021).

[83] A. E. Cárcamo Hernández, S. F. King, H. Lee, and S. J. Rowley, Is it possible to explain the muon and electron $g - 2$ in a $Z\prime$ model?, Phys. Rev. D **101,** 115016 (2020).

[84] A. Bodas, R. Coy, and S. J. D. King, Solving the electron and muon $g - 2$ anomalies in Z' models, Eur. Phys. J. C **81,** 1065 (2021).

[85] T. A. Chowdhury and S. Saad, Non-Abelian vector dark matter and lepton $g - 2$, J. Cosmol. Astropart. Phys. 10 (2021) 014.

[86] A. E. C. Hernández, S. Kovalenko, M. Maniatis, and I. Schmidt, Fermion mass hierarchy and $g - 2$ anomalies in an extended 3HDM Model, J. High Energy Phys. 10 (2021) 036.

[87] C.-H. Chen and T. Nomura, Electron and muon $g - 2$, radiative neutrino mass, and $\ell' \to \ell\gamma$ in a $U(1)_{e-\mu}$ model, Nucl. Phys. **B964,** 115314 (2021).

[88] L. Calibbi, M. L. López-Ibáñez, A. Melis, and O. Vives, Muon and electron $g - 2$ and lepton masses in flavor models, J. High Energy Phys. 06 (2020) 087.

[89] P. Anastasopoulos, K. Kaneta, E. Kiritsis, and Y. Mambrini, Anomalous and axial Z' contributions to $g - 2$, J. High Energy Phys. 02 (2023) 051.

[90] J.-L. Yang, T.-F. Feng, and H.-B. Zhang, Electron and muon $(g - 2)$ in the B-LSSM, J. Phys. G **47,** 055004 (2020).

[91] M. Badziak and K. Sakurai, Explanation of electron and muon $g - 2$ anomalies in the MSSM, J. High Energy Phys. 10 (2019) 024.

[92] M. Endo and W. Yin, Explaining electron and muon $g - 2$ anomaly in SUSY without lepton-flavor mixings, J. High Energy Phys. 08 (2019) 122.

[93] B. Dutta and Y. Mimura, Electron $g - 2$ with flavor violation in MSSM, Phys. Lett. B **790,** 563 (2019).

[94] H. Banerjee, B. Dutta, and S. Roy, Supersymmetric gauged $U(1)_{L_\mu - L_\tau}$ model for electron and muon $(g - 2)$ anomaly, J. High Energy Phys. 03 (2021) 211.

[95] M. Frank, Y. Hiçyılmaz, S. Mondal, O. Özdal, and C. S. Ün, Electron and muon magnetic moments and implications for dark matter and model characterisation in non-universal U(1)' supersymmetric models, J. High Energy Phys. 10 (2021) 063.

[96] S. Li, Y. Xiao, and J. M. Yang, Can electron and muon $g - 2$ anomalies be jointly explained in SUSY?, Eur. Phys. J. C **82,** 276 (2022).

[97] S. Li, Y. Xiao, and J. M. Yang, Constraining CP-phases in SUSY: An interplay of muon/electron $g - 2$ and electron EDM, Nucl. Phys. **B974,** 115629 (2022).

[98] M. I. Ali, M. Chakraborti, U. Chattopadhyay, and S. Mukherjee, Muon and electron $(g - 2)$ anomalies with non-holomorphic interactions in MSSM, Eur. Phys. J. C **83,** 60 (2023).

[99] S. Li, Z. Li, F. Wang, and J. M. Yang, Explanation of electron and muon $g - 2$ anomalies in AMSB, Nucl. Phys. **B983,** 115927 (2022).

[100] T. N. Dao, D. N. Le, and M. Mühlleitner, Leptonic anomalous magnetic and electric dipole moments in the CP-violating NMSSM with and without inverse seesaw mechanism, Eur. Phys. J. C **82,** 954 (2022).

[101] G. F. Giudice, P. Paradisi, and M. Passera, Testing new physics with the electron $g - 2$, J. High Energy Phys. 11 (2012) 113.

[102] X.-X. Dong, S.-M. Zhao, H.-B. Zhang, and T.-F. Feng, The two-loop corrections to lepton MDMs and EDMs in the EBLMSSM, J. Phys. G **47,** 045002 (2020).

[103] J. Cao, Y. He, J. Lian, D. Zhang, and P. Zhu, Electron and muon anomalous magnetic moments in the inverse seesaw extended NMSSM, Phys. Rev. D **104,** 055009 (2021).

[104] J. Aebischer, W. Dekens, E. E. Jenkins, A. V. Manohar, D. Sengupta, and P. Stoffer, Effective field theory interpretation of lepton magnetic and electric dipole moments, J. High Energy Phys. 07 (2021) 107.

[105] P. Fayet and S. Ferrara, Supersymmetry, Phys. Rep. **32,** 249 (1977).

[106] H. E. Haber and G. L. Kane, The search for supersymmetry: Probing physics beyond the standard model, Phys. Rep. **117,** 75 (1985).

[107] J. F. Gunion and H. E. Haber, Higgs bosons in supersymmetric models. 1., Nucl. Phys. **B272,** 1 (1986).

[108] A. Djouadi, The anatomy of electro-weak symmetry breaking. II. The Higgs bosons in the minimal super-symmetric model, Phys. Rep. **459**, 1 (2008).

[109] S. P. Martin, A supersymmetry primer, Adv. Ser. Dir. High Energy Phys. **18**, 1 (1998).

[110] G. Jungman, M. Kamionkowski, and K. Griest, Super-symmetric dark matter, Phys. Rep. **267**, 195 (1996).

[111] S. P. Martin and J. D. Wells, Muon anomalous magnetic dipole moment in supersymmetric theories, Phys. Rev. D **64**, 035003 (2001).

[112] F. Domingo and U. Ellwanger, Constraints from the muon $g - 2$ on the parameter space of the NMSSM, J. High Energy Phys. 07 (2008) 079.

[113] T. Moroi, The Muon anomalous magnetic dipole moment in the minimal supersymmetric Standard Model, Phys. Rev. D **53**, 6565 (1996).

[114] W. Hollik, J. I. Illana, S. Rigolin, and D. Stockinger, One loop MSSM contribution to the weak magnetic dipole moments of heavy fermions, Phys. Lett. B **416**, 345 (1998).

[115] P. Athron, M. Bach, H. G. Fargnoli, C. Gnendiger, R. Greifenhagen, J.-h. Park, S. Paßehr, D. Stöckinger, H. Stöckinger-Kim, and A. Voigt, GM2Calc: Precise MSSM prediction for $(g - 2)$ of the muon, Eur. Phys. J. C **76**, 62 (2016).

[116] M. Endo, K. Hamaguchi, S. Iwamoto, and T. Kitahara, Supersymmetric interpretation of the muon g–2 anomaly, J. High Energy Phys. 07 (2021) 075.

[117] D. Stockinger, The muon magnetic moment and super-symmetry, J. Phys. G **34**, R45 (2007).

[118] A. Czarnecki and W. J. Marciano, The Muon anomalous magnetic moment: A Harbinger for "new physics", Phys. Rev. D **64**, 013014 (2001).

[119] J. Cao, Z. Heng, D. Li, and J. M. Yang, Current exper-imental constraints on the lightest Higgs boson mass in the constrained MSSM, Phys. Lett. B **710**, 665 (2012).

[120] Z. Kang, $H_{u,d}$-messenger couplings address the μ/B_μ and $A_t/m^2_{H_u}$ problem and $(g - 2)_\mu$ puzzle, arXiv:1610.06024.

[121] B. Zhu, R. Ding, and T. Li, Higgs mass and muon anomalous magnetic moment in the MSSM with gauge-gravity hybrid mediation, Phys. Rev. D **96**, 035029 (2017).

[122] T. T. Yanagida and N. Yokozaki, Muon $g - 2$ in MSSM gauge mediation revisited, Phys. Lett. B **772**, 409 (2017).

[123] K. Hagiwara, K. Ma, and S. Mukhopadhyay, Closing in on the chargino contribution to the muon $g - 2$ in the MSSM: Current LHC constraints, Phys. Rev. D **97**, 055035 (2018).

[124] P. Cox, C. Han, and T. T. Yanagida, Muon $g - 2$ and dark matter in the minimal supersymmetric standard model, Phys. Rev. D **98**, 055015 (2018).

[125] H. M. Tran and H. T. Nguyen, GUT-inspired MSSM in light of muon $g - 2$ and LHC results at $\sqrt{s} = 13$ TeV, Phys. Rev. D **99**, 035040 (2019).

[126] B. P. Padley, K. Sinha, and K. Wang, Natural supersym-metry, muon $g - 2$, and the last crevices for the top squark, Phys. Rev. D **92**, 055025 (2015).

[127] A. Choudhury, L. Darmé, L. Roszkowski, E. M. Sessolo, and S. Trojanowski, Muon $g - 2$ and related phenomenol-ogy in constrained vector-like extensions of the MSSM, J. High Energy Phys. 05 (2017) 072.

[128] N. Okada and H. M. Tran, 125 GeV Higgs boson mass and muon $g - 2$ in 5D MSSM, Phys. Rev. D **94**, 075016 (2016).

[129] X. Du and F. Wang, NMSSM from alternative deflection in generalized deflected anomaly mediated SUSY breaking, Eur. Phys. J. C **78**, 431 (2018).

[130] X. Ning and F. Wang, Solving the muon $g - 2$ anomaly within the NMSSM from generalized deflected AMSB, J. High Energy Phys. 08 (2017) 089.

[131] K. Wang, F. Wang, J. Zhu, and Q. Jie, The semi-constrained NMSSM in light of muon $g - 2$, LHC, and dark matter constraints, Chin. Phys. C **42**, 103109 (2018).

[132] J.-L. Yang, T.-F. Feng, Y.-L. Yan, W. Li, S.-M. Zhao, and H.-B. Zhang, Lepton-flavor violation and two loop electro-weak corrections to $(g - 2)_\mu$ in the B-L symmetric SSM, Phys. Rev. D **99**, 015002 (2019).

[133] C.-X. Liu, H.-B. Zhang, J.-L. Yang, S.-M. Zhao, Y.-B. Liu, and T.-F. Feng, Higgs boson decay $h \rightarrow Z\gamma$ and muon magnetic dipole moment in the $\mu\nu$SSM, J. High Energy Phys. 04 (2020) 002.

[134] J. Cao, J. Lian, L. Meng, Y. Yue, and P. Zhu, Anomalous muon magnetic moment in the inverse seesaw extended next-to-minimal supersymmetric standard model, Phys. Rev. D **101**, 095009 (2020).

[135] W. Ke and P. Slavich, Higgs-mass constraints on a super-symmetric solution of the muon $g - 2$ anomaly, Eur. Phys. J. C **82**, 89 (2022).

[136] J. L. Lamborn, T. Li, J. A. Maxin, and D. V. Nanopoulos, Resolving the $(g - 2)_\mu$ discrepancy with $\mathcal{F} - SU(5)$ in-tersecting D-branes, J. High Energy Phys. 11 (2021) 081.

[137] Y. Nakai, M. Reece, and M. Suzuki, Supersymmetric alignment models for $(g - 2)_\mu$, J. High Energy Phys. 10 (2021) 068.

[138] J. S. Kim, D. E. Lopez-Fogliani, A. D. Perez, and R. R. de Austri, The new $(g - 2)_\mu$ and right-handed sneutrino dark matter, Nucl. Phys. **B974**, 115637 (2022).

[139] Z. Li, G.-L. Liu, F. Wang, J. M. Yang, and Y. Zhang, Gluino-SUGRA scenarios in light of FNAL muon $g - 2$ anomaly, J. High Energy Phys. 12 (2021) 219.

[140] W. Altmannshofer, S. A. Gadam, S. Gori, and N. Hamer, Explaining $(g - 2)_\mu$ with Multi-TeV sleptons, J. High Energy Phys. 07 (2021) 118.

[141] H. Baer, V. Barger, and H. Serce, Anomalous muon magnetic moment, supersymmetry, naturalness, LHC search limits and the landscape, Phys. Lett. B **820**, 136480 (2021).

[142] M. Chakraborti, L. Roszkowski, and S. Trojanowski, GUT-constrained supersymmetry and dark matter in light of the new $(g - 2)_\mu$ determination, J. High Energy Phys. 05 (2021) 252.

[143] A. Aboubrahim, M. Klasen, and P. Nath, What the Fermilab muon $g - 2$ experiment tells us about discovering supersymmetry at high luminosity and high energy up-grades to the LHC, Phys. Rev. D **104**, 035039 (2021).

[144] S. Iwamoto, T. T. Yanagida, and N. Yokozaki, Wino-Higgsino dark matter in MSSM from the $g - 2$ anomaly, Phys. Lett. B **823**, 136768 (2021).

[145] M. Chakraborti, S. Heinemeyer, and I. Saha, The new "MUON G-2" result and supersymmetry, Eur. Phys. J. C **81**, 1114 (2021).

[146] J. Cao, J. Lian, Y. Pan, D. Zhang, and P. Zhu, Improved $(g-2)_\mu$ measurement and singlino dark matter in μ-term extended $\mathbb{Z}_3$-NMSSM, J. High Energy Phys. 09 (2021) 175.

[147] W. Yin, Muon $g-2$ anomaly in anomaly mediation, J. High Energy Phys. 06 (2021) 029.

[148] H.-B. Zhang, C.-X. Liu, J.-L. Yang, and T.-F. Feng, Muon anomalous magnetic dipole moment in the $\mu\nu$SSM, Chin. Phys. C **46**, 093107 (2022).

[149] M. Ibe, S. Kobayashi, Y. Nakayama, and S. Shirai, Muon $g-2$ in gauge mediation without SUSY CP problem, J. High Energy Phys. 07 (2021) 098.

[150] C. Han, Muon $g-2$ and CP violation in MSSM, arXiv:2104.03292.

[151] F. Wang, L. Wu, Y. Xiao, J. M. Yang, and Y. Zhang, GUT-scale constrained SUSY in light of new muon $g-2$ measurement, Nucl. Phys. **B970**, 115486 (2021).

[152] M.-D. Zheng and H.-H. Zhang, Studying the $b \to s\ell + \ell$-anomalies and $(g-2)_\mu$ in R-parity violating MSSM framework with the inverse seesaw mechanism, Phys. Rev. D **104**, 115023 (2021).

[153] M. Chakraborti, S. Heinemeyer, I. Saha, and C. Schappacher, $(g-2)_\mu$ and SUSY dark matter: Direct detection and collider search complementarity, Eur. Phys. J. C **82**, 483 (2022).

[154] A. Aboubrahim, M. Klasen, P. Nath, and R. M. Syed, Tests of gluino-driven radiative breaking of the electroweak symmetry at the LHC, in *Proceedings of the 10th International Conference on New Frontiers in Physics* (2021), arXiv:2112.04986.

[155] K. Wang and J. Zhu, A smuon in the NMSSM confronted with the muon $g-2$ and SUSY searches, Chin. Phys. C **47**, 013107 (2023).

[156] M. Chakraborti, S. Heinemeyer, and I. Saha, Improved $(g-2)_\mu$ measurements and supersymmetry, Eur. Phys. J. C **80**, 984 (2020).

[157] S. Baum, M. Carena, N. R. Shah, and C. E. M. Wagner, The tiny $(g-2)$ muon wobble from small-μ supersymmetry, J. High Energy Phys. 01 (2022) 025.

[158] J. Cao, J. Lian, Y. Pan, Y. Yue, and D. Zhang, Impact of recent $(g-2)_\mu$ measurement on the light CP-even Higgs scenario in general next-to-minimal supersymmetric standard model, J. High Energy Phys. 03 (2022) 203.

[159] J. Cao, F. Li, J. Lian, Y. Pan, and D. Zhang, Impact of LHC probes of SUSY and recent measurement of $(g-2)_\mu$ on $\mathbb{Z}_3$-NMSSM, Sci. China Phys. Mech. Astron. **65**, 291012 (2022).

[160] F. Domingo, U. Ellwanger, and C. Hugonie, M_W, Dark matter and a_μ in the NMSSM, Eur. Phys. J. C **82**, 1074 (2022).

[161] J. Cao, X. Jia, L. Meng, Y. Yue, and D. Zhang, Status of the singlino-dominated dark matter in general next-to-minimal supersymmetric Standard Model, J. High Energy Phys. 03 (2023) 198.

[162] Y. He, X. Jia, L. Meng, Y. Yue, and D. Zhang, Impact of recent measurement of $(g-2)_\mu$, LHC search for supersymmetry, and LZ experiment on minimal supersymmetric standard model, arXiv:2303.02360.

[163] J. Aalbers *et al.* (LZ Collaboration), First Dark Matter Search Results from the LUX-ZEPLIN (LZ) Experiment, Phys. Rev. Lett. **131**, 041002 (2023).

[164] G. Aad *et al.* (ATLAS Collaboration), Search for electroweak production of charginos and sleptons decaying into final states with two leptons and missing transverse momentum in $\sqrt{s} = 13$ TeV pp collisions using the ATLAS detector, Eur. Phys. J. C **80**, 123 (2020).

[165] G. Aad *et al.* (ATLAS Collaboration), Search for chargino–neutralino pair production in final states with three leptons and missing transverse momentum in $\sqrt{s} = 13$ TeV pp collisions with the ATLAS detector, Eur. Phys. J. C **81**, 1118 (2021).

[166] A. M. Sirunyan *et al.* (CMS Collaboration), Search for supersymmetry in final states with two oppositely charged same-flavor leptons and missing transverse momentum in proton-proton collisions at $\sqrt{s} = 13$ TeV, J. High Energy Phys. 04 (2021) 123.

[167] A. M. Sirunyan *et al.* (CMS Collaboration), Combined search for electroweak production of charginos and neutralinos in proton-proton collisions at $\sqrt{s} = 13$ TeV, J. High Energy Phys. 03 (2018) 160.

[168] A. M. Sirunyan *et al.* (CMS Collaboration), Search for electroweak production of charginos and neutralinos in multilepton final states in proton-proton collisions at $\sqrt{s} = 13$ TeV, J. High Energy Phys. 03 (2018) 166.

[169] M. Aaboud *et al.* (ATLAS Collaboration), Search for electroweak production of supersymmetric particles in final states with two or three leptons at $\sqrt{s} = 13$ TeV with the ATLAS detector, Eur. Phys. J. C **78**, 995 (2018).

[170] M. Aaboud *et al.* (ATLAS Collaboration), Search for chargino-neutralino production using recursive jigsaw reconstruction in final states with two or three charged leptons in proton-proton collisions at $\sqrt{s} = 13$ TeV with the ATLAS detector, Phys. Rev. D **98**, 092012 (2018).

[171] G. Aad *et al.* (ATLAS Collaboration), Search for direct production of electroweakinos in final states with one lepton, missing transverse momentum and a Higgs boson decaying into two b-jets in pp collisions at $\sqrt{s} = 13$ TeV with the ATLAS detector, Eur. Phys. J. C **80**, 691 (2020).

[172] M. Aaboud *et al.* (ATLAS Collaboration), Search for chargino and neutralino production in final states with a Higgs boson and missing transverse momentum at $\sqrt{s} = 13$ TeV with the ATLAS detector, Phys. Rev. D **100**, 012006 (2019).

[173] A. M. Sirunyan *et al.* (CMS Collaboration), Search for new phenomena in final states with two opposite-charge, same-flavor leptons, jets, and missing transverse momentum in pp collisions at $\sqrt{s} = 13$ TeV, J. High Energy Phys. 03 (2018) 076.

[174] A. M. Sirunyan *et al.* (CMS Collaboration), Search for supersymmetry with Higgs boson to diphoton decays using the razor variables at $\sqrt{s} = 13$ TeV, Phys. Lett. B **779**, 166 (2018).

[175] A. M. Sirunyan *et al.* (CMS Collaboration), Searches for pair production of charginos and top squarks in final states with two oppositely charged leptons in proton-proton collisions at $\sqrt{s} = 13$ TeV, J. High Energy Phys. 11 (2018) 079.

[176] M. Aaboud *et al.* (ATLAS Collaboration), Search for photonic signatures of gauge-mediated supersymmetry in 13 TeV pp collisions with the ATLAS detector, Phys. Rev. D **97**, 092006 (2018).

[177] G. Aad *et al.* (ATLAS Collaboration), Search for supersymmetry in events with four or more charged leptons in 139 fb^{-1} of $\sqrt{s} = 13$ TeV pp collisions with the ATLAS detector, J. High Energy Phys. 07 (2021) 167.

[178] G. Aad *et al.* (ATLAS Collaboration), Searches for electroweak production of supersymmetric particles with compressed mass spectra in $\sqrt{s} = 13$ TeV pp collisions with the ATLAS detector, Phys. Rev. D **101**, 052005 (2020).

[179] M. Aaboud *et al.* (ATLAS Collaboration), Search for electroweak production of supersymmetric states in scenarios with compressed mass spectra at $\sqrt{s} = 13$ TeV with the ATLAS detector, Phys. Rev. D **97**, 052010 (2018).

[180] A. M. Sirunyan *et al.* (CMS Collaboration), Search for new physics in events with two soft oppositely charged leptons and missing transverse momentum in proton-proton collisions at $\sqrt{s} = 13$ TeV, Phys. Lett. B **782**, 440 (2018).

[181] A. M. Sirunyan *et al.* (CMS Collaboration), Search for supersymmetric partners of electrons and muons in proton-proton collisions at $\sqrt{s} = 13$ TeV, Phys. Lett. B **790**, 140 (2019).

[182] G. F. Giudice and A. Masiero, A natural solution to the mu problem in supergravity theories, Phys. Lett. B **206**, 480 (1988).

[183] A. Arvanitaki, M. Baryakhtar, X. Huang, K. van Tilburg, and G. Villadoro, The last vestiges of naturalness, J. High Energy Phys. 03 (2014) 022.

[184] J. A. Evans, Y. Kats, D. Shih, and M. J. Strassler, Toward full LHC coverage of natural supersymmetry, J. High Energy Phys. 07 (2014) 101.

[185] H. Baer, V. Barger, D. Mickelson, and M. Padeffke-Kirkland, SUSY models under siege: LHC constraints and electroweak fine-tuning, Phys. Rev. D **89**, 115019 (2014).

[186] U. Ellwanger, C. Hugonie, and A. Teixeira, The next-to-minimal supersymmetric standard model, Phys. Rep. **496**, 1 (2010).

[187] M. Maniatis, The next-to-minimal supersymmetric extension of the standard model reviewed, Int. J. Mod. Phys. A **25**, 3505 (2010).

[188] U. Ellwanger, A Higgs boson near 125 GeV with enhanced di-photon signal in the NMSSM, J. High Energy Phys. 03 (2012) 044.

[189] J.-J. Cao, Z.-X. Heng, J. M. Yang, Y.-M. Zhang, and J.-Y. Zhu, A SM-like Higgs near 125 GeV in low energy SUSY: A comparative study for MSSM and NMSSM, J. High Energy Phys. 03 (2012) 086.

[190] U. Ellwanger and A. M. Teixeira, NMSSM with a singlino LSP: Possible challenges for searches for supersymmetry at the LHC, J. High Energy Phys. 10 (2014) 113.

[191] J. Cao, Y. He, L. Shang, Y. Zhang, and P. Zhu, Current status of a natural NMSSM in light of LHC 13 TeV data and XENON-1T results, Phys. Rev. D **99**, 075020 (2019).

[192] S. Baum, M. Carena, N. R. Shah, and C. E. M. Wagner, Higgs portals for thermal dark matter. EFT perspectives and the NMSSM, J. High Energy Phys. 04 (2018) 069.

[193] N. Aghanim *et al.* (Planck Collaboration), Planck 2018 results. VI. Cosmological parameters, Astron. Astrophys. **641**, A6 (2020).

[194] E. Aprile *et al.* (XENON Collaboration), Dark Matter Search Results from a One Ton-Year Exposure of XENON1T, Phys. Rev. Lett. **121**, 111302 (2018).

[195] E. Aprile *et al.* (XENON Collaboration), Constraining the Spin-Dependent WIMP-Nucleon Cross Sections with XENON1T, Phys. Rev. Lett. **122**, 141301 (2019).

[196] F. Staub, SARAH, arXiv:0806.0538.

[197] F. Staub, SARAH 3.2: Dirac gauginos, UFO output, and more, Comput. Phys. Commun. **184**, 1792 (2013).

[198] F. Staub, SARAH 4: A tool for (not only SUSY) model builders, Comput. Phys. Commun. **185**, 1773 (2014).

[199] F. Staub, Exploring new models in all detail with SARAH, Adv. High Energy Phys. **2015**, 840780 (2015).

[200] W. Porod, SPheno, a program for calculating supersymmetric spectra, SUSY particle decays and SUSY particle production at $e^+ e^-$ colliders, Comput. Phys. Commun. **153**, 275 (2003).

[201] W. Porod and F. Staub, SPheno 3.1: Extensions including flavour, *CP*-phases and models beyond the MSSM, Comput. Phys. Commun. **183**, 2458 (2012).

[202] W. Porod, F. Staub, and A. Vicente, A flavor kit for BSM models, Eur. Phys. J. C **74**, 2992 (2014).

[203] G. Belanger, F. Boudjema, A. Pukhov, and A. Semenov, MicrOMEGAs: A program for calculating the relic density in the MSSM, Comput. Phys. Commun. **149**, 103 (2002).

[204] G. Belanger, F. Boudjema, C. Hugonie, A. Pukhov, and A. Semenov, Relic density of dark matter in the NMSSM, J. Cosmol. Astropart. Phys. 09 (2005) 001.

[205] G. Belanger, F. Boudjema, A. Pukhov, and A. Semenov, MicrOMEGAs 2.0: A program to calculate the relic density of dark matter in a generic model, Comput. Phys. Commun. **176**, 367 (2007).

[206] G. Belanger, F. Boudjema, A. Pukhov, and A. Semenov, MicrOMEGAs: A tool for dark matter studies, Nuovo Cimento Soc. Ital. Fis. **033N2C**, 111 (2010).

[207] G. Belanger, F. Boudjema, A. Pukhov, and A. Semenov, MicrOMEGAs_3: A program for calculating dark matter observables, Comput. Phys. Commun. **185**, 960 (2014).

[208] D. Barducci, G. Belanger, J. Bernon, F. Boudjema, J. Da Silva, S. Kraml, U. Laa, and A. Pukhov, Collider limits on new physics within MicrOMEGAs_4.3, Comput. Phys. Commun. **222**, 327 (2018).

[209] P. Bechtle, O. Brein, S. Heinemeyer, G. Weiglein, and K. E. Williams, HiggsBounds: Confronting arbitrary Higgs sectors with exclusion bounds from LEP and the Tevatron, Comput. Phys. Commun. **181**, 138 (2010).

[210] P. Bechtle, O. Brein, S. Heinemeyer, G. Weiglein, and K. E. Williams, HiggsBounds 2.0.0: Confronting neutral and charged Higgs sector predictions with exclusion bounds from LEP and the Tevatron, Comput. Phys. Commun. **182**, 2605 (2011).

[211] P. Bechtle, O. Brein, S. Heinemeyer, O. Stål, T. Stefaniak, G. Weiglein, and K. E. Williams, HiggsBounds – 4: Improved tests of extended Higgs sectors against exclusion bounds from LEP, the Tevatron and the LHC, Eur. Phys. J. C **74**, 2693 (2014).

[212] P. Bechtle, D. Dercks, S. Heinemeyer, T. Klingl, T. Stefaniak, G. Weiglein, and J. Wittbrodt, HiggsBounds-5: Testing Higgs sectors in the LHC 13 TeV era, Eur. Phys. J. C **80**, 1211 (2020).

[213] P. Bechtle, S. Heinemeyer, O. Sål, T. Stefaniak, and G. Weiglein, HiggsSignal: Confronting arbitrary Higgs sectors with measurements at the Tevatron and the LHC, Eur. Phys. J. C **74**, 2711 (2014).

[214] O. Stål and T. Stefaniak, Constraining extended Higgs sectors with HiggsSignal, Proc. Sci. EPS-HEP2013 (**2013**) 314.

[215] P. Bechtle, S. Heinemeyer, O. Stål, T. Stefaniak, and G. Weiglein, Probing the standard model with Higgs signal rates from the Tevatron, the LHC and a future ILC, J. High Energy Phys. 11 (2014) 039.

[216] P. Bechtle, S. Heinemeyer, T. Klingl, T. Stefaniak, G. Weiglein, and J. Wittbrodt, HiggsSignal-2: Probing new physics with precision Higgs measurements in the LHC 13 TeV era, Eur. Phys. J. C **81**, 145 (2021).

[217] F. Feroz, M. P. Hobson, and M. Bridges, MultiNest: An efficient and robust Bayesian inference tool for cosmology and particle physics, Mon. Not. R. Astron. Soc. **398**, 1601 (2009).

[218] M. Ackermann et al. (Fermi-LAT Collaboration), Searching for Dark Matter Annihilation from Milky Way Dwarf Spheroidal Galaxies with Six Years of Fermi Large Area Telescope Data, Phys. Rev. Lett. **115**, 231301 (2015).

[219] M. Tanabashi, K. Hagiwara, Hikasa et al. (Particle Data Group), Review of particle physics, Phys. Rev. D **98**, 030001 (2018).

[220] J. E. Camargo-Molina, B. O'Leary, W. Porod, and F. Staub, **Vevacious**: A tool for finding the global minima of one-loop effective potentials with many scalars, Eur. Phys. J. C **73**, 2588 (2013).

[221] W. Beenakker, R. Hopker, and M. Spira, PROSPINO: A program for the production of supersymmetric particles in next-to-leading order QCD, arXiv:hep-ph/9611232.

[222] C. K. Khosa, S. Kraml, A. Lessa, P. Neuhuber, and W. Waltenberger, SModelS database update v1.2.3, Lett. High Energy Phys. **2020**, 158 (2020).

[223] J. Alwall, M. Herquet, F. Maltoni, O. Mattelaer, and T. Stelzer, MadGraph 5: Going beyond, J. High Energy Phys. 06 (2011) 128.

[224] E. Conte, B. Fuks, and G. Serret, MadAnalysis 5, a user-friendly framework for collider phenomenology, Comput. Phys. Commun. **184**, 222 (2013).

[225] T. Sjöstrand, S. Ask, J. R. Christiansen, R. Corke, N. Desai, P. Ilten, S. Mrenna, S. Prestel, C. O. Rasmussen, and P. Z. Skands, An introduction to PYTHIA 8.2, Comput. Phys. Commun. **191**, 159 (2015).

[226] M. Drees, H. Dreiner, D. Schmeier, J. Tattersall, and J. S. Kim, CheckMATE: Confronting your favourite new physics model with LHC data, Comput. Phys. Commun. **187**, 227 (2015).

[227] D. Dercks, N. Desai, J. S. Kim, K. Rolbiecki, J. Tattersall, and T. Weber, CheckMATE 2: From the model to the limit, Comput. Phys. Commun. **221**, 383 (2017).

[228] J. S. Kim, D. Schmeier, J. Tattersall, and K. Rolbiecki, A framework to create customised LHC analyses within CheckMATE, Comput. Phys. Commun. **196**, 535 (2015).

[229] J. de Favereau, C. Delaere, P. Demin, A. Giammanco, V. Lemaître, A. Mertens, and M. Selvaggi (DELPHES 3 Collaboration), DELPHES 3, a modular framework for fast simulation of a generic collider experiment, J. High Energy Phys. 02 (2014) 057.

[230] F. Domingo, J. S. Kim, V. M. Lozano, P. Martin-Ramiro, and R. Ruiz de Austri, Confronting the neutralino and chargino sector of the NMSSM with the multilepton searches at the LHC, Phys. Rev. D **101**, 075010 (2020).

[231] K. Griest and D. Seckel, Three exceptions in the calculation of relic abundances, Phys. Rev. D **43**, 3191 (1991).

[232] ILC Collaboration, The international linear collider technical design report—volume 2: Physics, arXiv:1306.6352.

[233] M. Chakraborti, S. Heinemeyer, and I. Saha, Improved $(g-2)_\mu$ measurements and supersymmetry: Implications for e^+e^- colliders, arXiv:2105.06408.

[234] J. Cao, L. Meng, Y. Yue, H. Zhou, and P. Zhu, Suppressing the scattering of WIMP dark matter and nucleons in supersymmetric theories, Phys. Rev. D **101**, 075003 (2020).